Article

Electronic Structure of Six-Coordinate Iron(III)#Porphyrin NO Adducts: The Elusive Iron(III)#NO(radical) State and Its Influence on the Properties of These Complexes

V. K. K. Praneeth, Florian Paulat, Timothy C. Berto, Serena DeBeer George, Christian Na#ther, Corinne D. Sulok, and Nicolai Lehnert

J. Am. Chem. Soc., **2008**, 130 (46), 15288-15303 • DOI: 10.1021/ja801860u • Publication Date (Web): 23 October 2008

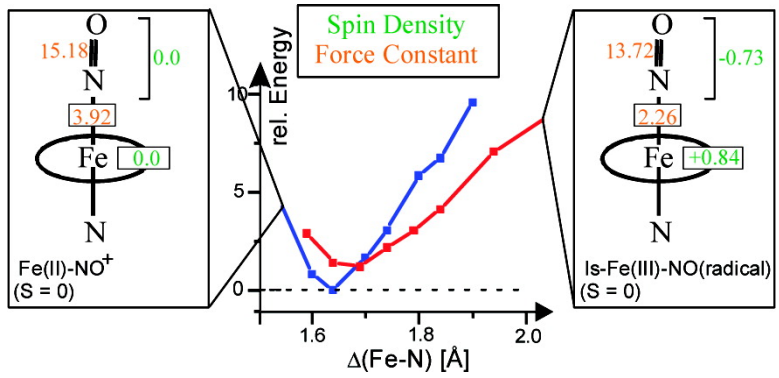

More About This Article

Additional resources and features associated with this article are available within the HTML version:

- Supporting Information
- Links to the 1 articles that cite this article, as of the time of this article download
- Access to high resolution figures
- Links to articles and content related to this article
- Copyright permission to reproduce figures and/or text from this article

View the Full Text HTML

J|A|C|S
ARTICLES

Published on Web 10/23/2008

Electronic Structure of Six-Coordinate Iron(III)−Porphyrin NO Adducts: The Elusive Iron(III)−NO(radical) State and Its Influence on the Properties of These Complexes

V. K. K. Praneeth,[†] Florian Paulat,[†] Timothy C. Berto,[†] Serena DeBeer George,[‡] Christian Näther,[§] Corinne D. Sulok,[†] and Nicolai Lehnert*[,†]

Department of Chemistry, University of Michigan, Ann Arbor, Michigan 48109, Stanford Synchrotron Radiation Laboratory, SLAC, Stanford University, Stanford, California 94309, and Institut für Anorganische Chemie, Christian-Albrechts-Universität Kiel, Olshausenstrasse 40, D-24098 Kiel, Germany

Received March 12, 2008; E-mail: lehnertn@umich.edu

Abstract: This paper investigates the interaction between five-coordinate ferric hemes with bound axial imidazole ligands and nitric oxide (NO). The corresponding model complex, [Fe(TPP)(MI)(NO)](BF$_4$) (MI = 1-methylimidazole), is studied using vibrational spectroscopy coupled to normal coordinate analysis and density functional theory (DFT) calculations. In particular, nuclear resonance vibrational spectroscopy is used to identify the Fe−N(O) stretching vibration. The results reveal the usual Fe(II)−NO$^+$ ground state for this complex, which is characterized by strong Fe−NO and N−O bonds, with Fe−NO and N−O force constants of 3.92 and 15.18 mdyn/Å, respectively. This is related to two strong π back-bonds between Fe(II) and NO$^+$. The alternative ground state, low-spin Fe(III)−NO(radical) ($S = 0$), is then investigated. DFT calculations show that this state exists as a stable minimum at a surprisingly low energy of only ∼1−3 kcal/mol above the Fe(II)−NO$^+$ ground state. In addition, the Fe(II)−NO$^+$ potential energy surface (PES) crosses the low-spin Fe(III)−NO(radical) energy surface at a very small elongation (only 0.05−0.1 Å) of the Fe−NO bond from the equilibrium distance. This implies that ferric heme nitrosyls with the latter ground state might exist, particularly with axial thiolate (cysteinate) coordination as observed in P450-type enzymes. Importantly, the low-spin Fe(III)−NO(radical) state has very different properties than the Fe(II)−NO$^+$ state. Specifically, the Fe−NO and N−O bonds are distinctively weaker, showing Fe−NO and N−O force constants of only 2.26 and 13.72 mdyn/Å, respectively. The PES calculations further reveal that the thermodynamic weakness of the Fe−NO bond in ferric heme nitrosyls is an intrinsic feature that relates to the properties of the high-spin Fe(III)−NO(radical) ($S = 2$) state that appears at low energy and is dissociative with respect to the Fe−NO bond. Altogether, release of NO from a six-coordinate ferric heme nitrosyl requires the system to pass through at least three different electronic states, a process that is remarkably complex and also unprecedented for transition-metal nitrosyls. These findings have implications not only for heme nitrosyls but also for group-8 transition-metal(III) nitrosyls in general.

Introduction

Nitric oxide (NO) is a poisonous gas that is, however, of great biological significance. Therefore, in 1992 it was chosen as the "molecule of the year" by the magazine *Science*.[1] In the years since then, further research has shown that NO plays a key role in nerve-signal transduction, vasodilation, blood clotting, and immune response by white blood cells.[2,3] NO is produced in vivo by the nitric oxide synthase (NOS) family of enzymes.[4] Cardiovascular regulation by NO (produced by endothelial (e-) NOS) is then mediated by soluble guanylate cyclase.[3d,5] The role of nitric oxide in vasodilation is exploited by certain blood-sucking insects whose bites inject NO into their

[†] University of Michigan.
[‡] Stanford University.
[§] Christian-Albrechts-Universität Kiel.

(1) Culotta, E.; Koshland, D. E. *Science* **1992**, *258*, 1862–1865.
(2) (a) Moncada, S.; Palmer, R. M.; Higgs, E. A. *Pharmacol. Rev.* **1991**, *43*, 109–142. (b) Snyder, S. H. *Science* **1992**, *257*, 494–496. (c) Butler, A. R.; Williams, D. L. H. *Chem. Soc. Rev.* **1993**, 233–241. (d) Bredt, D. S.; Snyder, S. H. *Annu. Rev. Biochem.* **1994**, *63*, 175–195. (e) Lancaster, J. R., Jr. In *Encyclopedia of Inorganic Chemistry*; Bruce, R. B., Ed.; Wiley: Chichester, U.K., 1994. (f) *Methods in Nitric Oxide Research*; Feelisch, M., Stamler, J. S., Eds.; Wiley: Chichester, U.K., 1996. (g) Cooper, C. E. *Biochim. Biophys. Acta* **1999**, *1411*, 290–309.
(3) (a) Stamler, J. S.; Singel, D. J.; Loscalzo, J. *Science* **1992**, *258*, 1898–1902. (b) Hughes, M. N. *Biochim. Biophys. Acta* **1999**, *1411*, 263–272. (c) *Nitric Oxide: Biology and Pathobiology*; Ignarro, L., Ed.; Academic Press: San Diego, CA, 2000. (d) Ballou, D. P.; Zhao, Y.; Brandish, P. E.; Marletta, M. A. *Proc. Natl. Acad. Sci. U.S.A.* **2002**, *99*, 12097–12101. (e) Feelisch, M.; Rassaf, T.; Mnaimneh, S.; Singh, N.; Bryan, N. S.; Jourd'Heuil, D.; Kelm, M. *FASEB J.* **2002**, *16*, 1775–1785. (f) McCleverty, J. A. *Chem. Rev.* **2004**, *104*, 403–418. (g) Farmer, P. J.; Sulc, F. *J. Inorg. Biochem.* **2005**, *99*, 166–184. (h) Boon, E. M.; Marletta, M. A. *J. Inorg. Biochem.* **2005**, *99*, 892–902. (i) Luchsinger, B. P.; Rich, E. N.; Yan, Y.; Williams, E. M.; Stamler, J. S.; Singel, D. J. *J. Inorg. Biochem.* **2005**, *99*, 912–921.
(4) (a) Stuehr, D. J. *Annu. Rev. Pharmacol. Toxicol.* **1997**, *37*, 339–359. (b) Poulos, T. L.; Li, H.; Raman, C. S. *Curr. Opin. Chem. Biol.* **1999**, *3*, 131–137. (c) Li, H.; Poulos, T. L. *J. Inorg. Biochem.* **2005**, *99*, 293–305. (d) Rousseau, D. L.; Li, D.; Couture, M.; Yeh, S.-R. *J. Inorg. Biochem.* **2005**, *99*, 306–323.

 10.1021/ja801860u CCC: $40.75

victims using small NO-carrier proteins, the so-called nitrophorins (Np's).[6] Finally, nitric oxide is an intermediate in dissimilatory denitrification.[7] In a number of these proteins, ferric heme NO adducts occur as intermediates of catalysis or as enzyme−product complexes. The observed biological Fe(III)−porphyrin NO adducts can be divided into two classes, depending on the nature of the axial ligand coordinated *trans* to NO, which is either an N-donor ligand such as histidine (His) or a thiolate cysteinate (Cys). In cytochrome cd_1 nitrite reductase (NiR), a six-coordinate (6C) ferric heme NO complex with axial His coordination is observed as the enzyme−product complex.[8] The nitrophorins from *Rhodnius prolixus* (rNp1−rNp4) contain ferric heme centers with axial His ligation.[6a,c] These Np proteins reversibly bind NO and release it in the victim's tissue. Ferric heme NO adducts with axial Cys coordination occur at the end of the catalytic cycle of the NOS enzymes. Recently, corresponding nitrophorins containing an axial Cys ligand have also been identified.[6c] Finally, the ferric form of fungal NO reductase (P450nor) is catalytically active and binds NO to form an Fe(III)−porphyrin NO adduct with axial Cys coordination (the enzyme−substrate complex).[9,10]

In the so-called Enemark−Feltham scheme, the Fe(III)−porphyrin NO adducts are classified as $\{FeNO\}^6$ complexes, where the exponent "6" refers to the number of Fe d electrons plus the unpaired electron of NO.[11] The electronic structure of the $\{FeNO\}^6$ heme complexes with axial N-donor coordination has in general been described[8] as Fe(II)−NO^+ in agreement with $\{RuNO\}^6$ systems, in which this electronic structure has been observed previously and studied extensively.[12] Hence, the Fe−NO interaction in these complexes is dominated by π back-bonding from two t_2-type d orbitals ("d_π" orbitals) of low-spin Fe(II) into the unoccupied π^* orbitals of NO^+. This bonding description is analogous to that for the isoelectronic Fe(II)−CO complexes. Crystal structures of Fe(III)−porphyrin NO model complexes are known for five-coordinate (5C) [Fe(OEP)(NO)](ClO_4) (OEP = octaethylporphyrin)[13] and six-coordinate (6C) [Fe(OEP)(L)(NO)](ClO_4) (L = neutral N-donor ligands).[14] These complexes show linear Fe−N−O units and extremely short Fe−NO bond lengths of 1.63−1.65 Å, in agreement with the Fe(II)−NO^+ description. The N−O stretching vibrations in these complexes are usually found in the 1900 cm^{-1} region (Table 1), which also reflects the coordinated NO^+. Hence, it was believed for some time that the bonding description of $\{FeNO\}^6$ is fully analogous to that of Fe(II)−CO.

Table 1. Vibrational Properties of Ferric Heme NO Adducts in Proteins and Model Complexes

complex	ν(N−O) [cm^{-1}]	ν(Fe−NO) [cm^{-1}]	refs
P450cam−NO	1806	528	9c, 41
P450cam−NO + adamantone	1818	520	9c, 41
SR−NO[a]	1828	510	58
P450nor−NO	1851	530	9c
CPO−NO[a]	1868	538	9c, 59
iNOS−NO		537	4d
[Fe(OEP)(NO)](ClO_4)[b]	1868/1838	611/600	13, 16a
HRP−NO[a]	1903	604	40, 60
NorBC−NO[a]	1904	594	61
rNp1−NO	1917	591	6b, 45
hHO-1−NO[a]	1918	596	62
[Fe(OEP)(MI)(NO)](ClO_4)	1921	−	14a
Hb−NO[a]	1925	594	63, 40
Mb−NO[a]	1927	595	64, 40
[Fe(TPP)(HO-*i*-C_5H_{11})(NO)](ClO_4)	1935	−	14d

[a] SR = picket fence porphyrin model complex with axial thiolate ligand; CPO = chloroperoxidase; HRP = horseradish peroxidase; NorBC = bacterial NOR; hHO-1 = human heme oxygenase-1; Hb = hemoglobin; Mb = myoglobin. [b] Data are given for the chloroform solvate and the corresponding solvent-free complex, respectively.

However, recent density functional theory (DFT) studies found that the N−O and Fe−NO stretching vibrations in Fe(III)−porphyrin NO adducts show a direct correlation upon porphyrin ring substitution, which is in contrast to the behavior of Fe(II)−porphyrin CO complexes.[15] Therefore, *further contributions to the Fe−NO bond in addition to the strong π back-bond must exist in these complexes*.[16] Related to this, axial thiolate coordination to $\{FeNO\}^6$ in heme proteins and model complexes is known to induce bent Fe−N−O units ($\angle$(Fe−N−O) = 161−165°),[17,9b,18] and lower N−O stretching frequencies (1800−1850 cm^{-1}). In a recent study, these differences have been attributed to a *trans* effect of the thiolate on the bound NO that leads to the occupation of an Fe−N−O σ antibonding orbital, which is responsible for the bending of the Fe−N−O unit and the weakening of the Fe−NO and N−O bonds.[19] In addition to these slight variations in the "classic" π back-bonding

(5) (a) Garbers, D. L.; Lowe, D. G. *J. Biol. Chem.* **1994**, *269*, 30741–30744. (b) Zhao, Y.; Hoganson, C.; Babcock, G. T.; Marletta, M. A. *Biochemistry* **1998**, *37*, 12458–12464. (c) Karow, D. S.; Pan, D.; Tran, R.; Pellicena, P.; Presley, A.; Mathies, R. A.; Marletta, M. A. *Biochemistry* **2004**, *43*, 10203–10211. (d) Gilles-Gonzalez, M.-A.; Gonzales, G. *J. Inorg. Biochem.* **2005**, *99*, 1–22.

(6) (a) Ribeiro, J. M. C.; Hazzard, J. M. H.; Nussenzveig, R. H.; Champagne, D. E.; Walker, F. A. *Science* **1993**, *260*, 539–541. (b) Ding, X. D.; Weichsel, A.; Andersen, J. F.; Shokhireva, T. K.; Balfour, C.; Pierik, A. J.; Averill, B. A.; Montfort, W. R.; Walker, F. A. *J. Am. Chem. Soc.* **1999**, *121*, 128–138. (c) Walker, F. A. *J. Inorg. Biochem.* **2005**, *99*, 216–236.

(7) (a) Ferguson, S. J. *Curr. Opin. Chem. Biol.* **1998**, *2*, 182–193. (b) Richardson, D. J.; Watmough, N. J. *Curr. Opin. Chem. Biol.* **1999**, *3*, 207–219. (c) Moura, I.; Moura, J. J. G. *Curr. Opin. Chem. Biol.* **2001**, *5*, 168–175.

(8) (a) Averill, B. A. *Chem. Rev.* **1996**, *96*, 2951–2964. (b) Wasser, I. M.; de Vries, S.; Moënne-Loccoz, P.; Schröder, I.; Karlin, K. D. *Chem. Rev.* **2002**, *102*, 1201–1234.

(9) (a) Park, S.-Y.; Shimizu, H.; Adachi, S.-I.; Nakagawa, A.; Tanaka, I.; Nakahara, K.; Shoun, H.; Obayashi, E.; Nakamura, H.; Iizuka, T.; Shiro, Y. *Nat. Struct. Biol.* **1997**, *4*, 827–832. (b) Shimizu, H.; Park, S.-Y.; Gomi, Y.; Arakawa, H.; Nakamura, H.; Adachi, S.-I.; Obayashi, E.; Iizuka, T.; Shoun, H.; Shiro, Y. *J. Biol. Chem.* **2000**, *275*, 4816. (c) Obayashi, E.; Tsukamoto, K.; Adachi, S.-I.; Takahashi, S.; Nomura, M.; Iizuka, T.; Shoun, H.; Shiro, Y. *J. Am. Chem. Soc.* **1997**, *119*, 7807–7816. (d) Daiber, A.; Shoun, H.; Ullrich, V. *J. Inorg. Biochem.* **2005**, *99*, 185–193.

(10) (a) Shiro, Y.; Fujii, M.; Iizuka, T.; Adachi, S.-I.; Tsukamoto, K.; Nakahara, K.; Shoun, H. *J. Biol. Chem.* **1995**, *270*, 1617–1623. (b) Lehnert, N.; Praneeth, V. K. K.; Paulat, F. *J. Comput. Chem.* **2006**, *27*, 1338–1351.

(11) Enemark, J. H.; Feltham, R. D. *Coord. Chem. Rev.* **1974**, *13*, 339–406.

(12) (a) Bottomley, F. *Coord. Chem. Rev.* **1978**, *26*, 7–32, and references therein. (b) Paulat, F.; Kuschel, T.; Näther, C.; Praneeth, V. K. K.; Sander, O.; Lehnert, N. *Inorg. Chem.* **2004**, *43*, 6979–6994.

(13) Ellison, M. K.; Schulz, C. E.; Scheidt, W. R. *Inorg. Chem.* **2000**, *39*, 5102–5110.

(14) (a) Ellison, M. K.; Scheidt, W. R. *J. Am. Chem. Soc.* **1999**, *121*, 5210–5219. (b) Ellison, M. K.; Schulz, C. E.; Scheidt, W. R. *J. Am. Chem. Soc.* **2002**, *124*, 13833–13841. (c) Scheidt, W. R.; Lee, Y. J.; Hatano, K. *J. Am. Chem. Soc.* **1984**, *106*, 3191–3198. (d) Yi, G.-B.; Chen, L.; Khan, M. A.; Richter-Addo, G. B. *Inorg. Chem.* **1997**, *36*, 3876–3885.

(15) (a) Li, X.-Y.; Spiro, T. G. *J. Am. Chem. Soc.* **1988**, *110*, 6024–6033. (b) Ray, G. B.; Li, X.-Y.; Ibers, J. A.; Sessler, J. L.; Spiro, T. G. *J. Am. Chem. Soc.* **1994**, *116*, 162–176, and references therein.

(16) (a) Linder, D. P.; Rodgers, K. R.; Banister, J.; Wyllie, G. R. A.; Ellison, M. K.; Scheidt, W. R. *J. Am. Chem. Soc.* **2004**, *126*, 14136–14148. (b) Linder, D. P.; Rodgers, K. R. *Inorg. Chem.* **2005**, *44*, 1367–1380.

(17) Pant, K.; Crane, B. R. *Biochemistry* **2006**, *45*, 2537–2544.

(18) Xu, N.; Powell, D. R.; Cheng, L.; Richter-Addo, G. B. *Chem. Commun.* **2006**, 2030–2032.

(19) Paulat, F.; Lehnert, N. *Inorg. Chem.* **2007**, *46*, 1547–1549.

electronic structure model for $\{FeNO\}^6$, it has been pointed out by Walker[6c] that the $\{FeNO\}^6$ formalism leaves room for an even wider variation in electronic structure: the Fe(III)−porphyrin NO adducts could also exhibit an Fe(III)−NO(radical) electronic structure if the low-spin Fe(III) electron configuration is $[d_{xz}^2 d_{yz}^2 d_{xy}^1]$, which requires a ruffled porphyrin ring; in this electron configuration, the unpaired electrons of low-spin Fe(III) and NO are antiferromagnetically coupled. This would be advantageous for the nitrophorins because it would prevent the autoxidation reaction of Fe(II)−NO^+ complexes,[20] which ultimately leads to ferrous NO adducts and hence to deactivation of the proteins as NO carriers. However, it is not known whether the bent Fe−N−O unit could in fact be caused by an Fe(III)−NO(radical) electronic structure. In order to understand the functioning of the nitrophorins and the nature of ferric heme−NO interactions in general, it is necessary to elucidate the electronic structures of the Fe(III)−porphyrin NO adducts in detail. The established Fe(II)−NO^+ and elusive Fe(III)−NO(radical) electronic structures lead to very different reactivities. In addition, the formation of an Fe(II)−NO^+ complex from ferric heme and NO requires an NO-to-Fe(III) electron transfer. However, not much is known about the energetics and the mechanism of complex formation in these systems.

In this study, the mechanism and energy landscape of NO binding to ferric hemes and the possible variation in electronic structure of ferric heme nitrosyls are investigated in detail. Since well-characterized ferric heme NO model complexes are surprisingly rare, we have prepared the 6C model system [Fe(TPP)(MI)(NO)](BF_4) (**1**; TPP = tetraphenylporphyrin, MI = 1-methylimidazole) and characterized this compound using vibrational spectroscopy coupled to isotope substitution. In particular, nuclear resonance vibrational spectroscopy (NRVS) was applied for the first time to a ferric heme nitrosyl in order to identify the Fe−NO stretching vibration of **1**. The vibrational data were then analyzed using our quantum chemistry centered normal coordinate analysis (QCC-NCA),[21b] and force constants for the Fe−NO and N−O bonds were determined. We have also extended our QCC-NCA package to calculate NRVS intensities directly from the NCA results. In this way, the first detailed analysis of the Fe−N−O vibrations in a 6C Fe(III)−porphyrin NO model complex is provided in this paper. The electronic structure of ferric heme nitrosyls was then evaluated and compared to that of corresponding ferrous complexes that we have recently investigated.[21,10b] This allowed the different complex stabilities and Fe−NO bond strengths in these systems to be rationalized, especially the lability of the Fe−NO bond in the ferric case. Finally, the binding of NO to ferric hemes was explored using potential energy surface (PES) calculations in order to elucidate (a) the relative stabilities of Fe(II)−NO^+ and Fe(III)−NO(radical) electronic states, (b) the mechanism of NO binding to ferric heme (i.e., the NO-to-Fe(III) electron transfer upon coordination of NO), and (c) the surprisingly large Fe−NO force constant in ferric hemes. It is demonstrated that the elusive Fe(III)−NO(radical) state appears as a minimum on the PES. The biological implications of these results are discussed.

Experimental and Computational Procedures

Syntheses. Reactions were performed by applying Schlenk techniques using carefully purified solvents. NO gas was purified by passing it first through an ascarite II column (NaOH on silica gel) and then through a cold trap at −60 to −70 °C to exclude higher nitrogen oxide impurities. $^{15}N^{18}O$-labeled compounds were synthesized using $^{15}N^{18}O$ gas (Sigma-Aldrich).

Syntheses of Precursors. Tetraphenylporphyrin (H_2TPP),[22] [Fe(TPP)Cl],[23] [Fe(TPP)ClO_4],[24] and [Fe(TPP)]$_2$O [25] were synthesized and purified as previously reported.

Synthesis of the Ferric NO Adduct [Fe(TPP)(MI)(NO)](BF_4) (1). A sample of [Fe^{III}(TPP)ClO_4] (100 mg, 0.13 mmol) and KBF_4 (160 mg, 1.3 mmol) was placed in a 100 mL Schlenk flask. The flask was purged three times with argon, and 20 mL of $CHCl_3$ was added. This heterogeneous reaction mixture was stirred at room temperature for ∼2 h and then filtered. The obtained filtrate, [Fe^{III}(TPP)(BF_4)] (the precursor complex), was collected in a 100 mL Schlenk flask, and 1-methylimidazole (MI, 10 μL, 0.13 mmol) was added. NO gas was then passed through the stirred solution for 10 min, and 15 mL of *n*-hexane was slowly added to the reaction mixture, which was then stored at −20 °C for 2 days. The precipitate was filtered off and obtained as a microcrystalline solid. The IR spectrum showed ν(N−O) at 1896 cm^{-1}, indicative of the formation of **1**. Yield: 92 mg (86%).

Synthesis of [Fe(TPP)(NO)(NO_2)] (2). [FeTPP]$_2$O (0.1 g, 0.074 mmol) was dissolved in 18 mL of $CHCl_3$ in a 100 mL Schlenk flask under an argon atmosphere. The solution was stirred for a few minutes, and then excess nitric oxide was added. Next, 0.2 mL of air was injected into the flask. The resulting solution was allowed to stir under the NO/O_2 atmosphere for 1 h. Finally, 22 mL of *n*-hexane was added, and the obtained precipitate was filtered off and stored under an argon atmosphere in a freezer. Yield: 86 mg (78%). IR [cm^{-1}]: ν(N−O), 1876; $\nu_{as}(NO_2)$, 1460; $\nu_s(NO_2)$, 1298.

Synthesis of [^{57}Fe(TPP)Cl].[26] In a Schlenk flask under an argon atmosphere, anhydrous HCl gas was bubbled slowly into a suspension of ^{57}Fe powder (1.00 g, 87.8 mmol; Cambridge Isotopes) in 50 mL of dry tetrahydrofuran (THF) at 0 °C. A white precipitate formed during the first hour and then dissolved after another hour, and the THF began to thicken, indicating the decomposition of THF to 4-chloro-1-butanol. After 5 h of reaction, argon was passed through the solution overnight to eliminate any residual HCl. The residual THF was distilled off, resulting in the formation of a dark-green gel-like substance. The 4-chloro-1-butanol was removed in vacuo to yield a green solid. This solid was washed with THF to yield a light-green solid, which was dried in vacuo. The obtained $^{57}FeCl_2$ was used without further purification in the metalation of H_2TPP to yield [^{57}Fe(TPP)Cl].[23]

Crystal Structure Determination. Single crystals of the ferric bis(thf)-coordinated precursor complex [Fe(TPP)(thf)$_2$](BF_4) (thf

(20) (a) Ehrenberg, A.; Szczepkowski, T. W. *Acta Chem. Scand.* **1960**, *14*, 1684–1692. (b) Hoshino, M.; Maeda, M.; Konishi, R.; Seki, H.; Ford, P. C. *J. Am. Chem. Soc.* **1996**, *118*, 5702–5707. (c) Fernandez, B. O.; Lorkovic, I. M.; Ford, P. C. *Inorg. Chem.* **2004**, *43*, 5393–5402. (d) Mǿller, J. K. S.; Skibsted, L. H. *Chem.−Eur. J.* **2004**, *10*, 2291–2300. (e) Lim, M. D.; Lorkovic, I. M.; Ford, P. C. *J. Inorg. Biochem.* **2005**, *99*, 151–165.

(21) (a) Praneeth, V. K. K.; Neese, F.; Lehnert, N. *Inorg. Chem.* **2005**, *44*, 2570–2572. (b) Praneeth, V. K. K.; Näther, C.; Peters, G.; Lehnert, N. *Inorg. Chem.* **2006**, *45*, 2795–2811. (c) Praneeth, V. K. K.; Haupt, E.; Lehnert, N. *J. Inorg. Biochem.* **2005**, *99*, 940–948. Erratum: Praneeth, V. K. K.; Haupt, E.; Lehnert, N. *J. Inorg. Biochem.* **2005**, *99*, 1744. (d) Lehnert, N. In *The Smallest Biomolecules: Perspectives on Heme−Diatomic Interactions*; Ghosh, A., Ed.; Elsevier: Amsterdam, 2008. (e) Paulat, F.; Berto, T. C.; DeBeer George, S.; Goodrich, L.; Praneeth, V. K. K.; Sulok, C. D.; Lehnert, N. *Inorg. Chem.*, in press.

(22) Adler, A. D.; Longo, F. R.; Finarrelli, J. D.; Goldmacher, J.; Assour, J.; Korsakoff, L. *J. Org. Chem.* **1967**, *32*, 476.

(23) Adler, A. D.; Longo, F. R.; Kampas, F.; Kim, J. *J. Inorg. Nucl. Chem.* **1970**, *32*, 2443–2445.

(24) Reed, C. A.; Mashiko, T.; Bently, P.; Kastner, M. E.; Scheidt, W. E.; Spartalian, K.; Lang, G. *J. Am. Chem. Soc.* **1979**, *101*, 2948–2958.

(25) Rai, B. K.; Durbin, S. M.; Prohofsky, E. W.; Sage, J. T.; Ellison, M. K.; Roth, A.; Scheidt, W. R.; Sturhahn, W.; Alp, E. E. *J. Am. Chem. Soc.* **2003**, *125*, 6927–6936.

(26) Aresta, M.; Nobile, C. F.; Petruzzelli, D. *Inorg. Chem.* **1977**, *16*, 1817–1818.

Table 2. Crystallographic Data for $[Fe^{III}(TPP)(thf)_2](BF_4)$

chemical formula	$C_{56}H_{52}BF_4FeN_4O_3$
formula weight	971.68
space group	$P\bar{1}$
a	10.6964(9) Å
b	13.4320(10) Å
c	18.7082(15) Å
α	78.173(9)°
β	86.379(10)°
γ	82.788(9)°
V	2608.1(4) Å^3
T	170 K
Z	2
D_{calcd}	1.237 Mg/m^3
μ	0.349 mm^{-1}
λ	0.71073 Å
measured reflections	21052
independent reflections	11889
R_{int}	0.0367
Observed reflections	8221
R1 $[I > 2\sigma(I)]^a$	0.0475
wR2 (all data)^b	0.1310

^{a} $R1 = \sum||F_o| - |F_c||/\sum|F_o|$. ^{b} $wR2 = \{\sum[w(F_o^2 - F_c^2)^2]/\sum[w(F_o^2)^2]\}^{1/2}$.

Table 3. Selected Bond Lengths and Angles for $[Fe^{III}(TPP)(thf)_2](BF_4)$

	Bond Lengths [Å]		
Fe(1)−N(1)	2.026(2)	Fe(1)−N(2)	2.031(2)
Fe(1)−N(3)	2.028(2)	Fe(1)−N(4)	2.031(2)
Fe(1)−O(1)	2.190(2)	Fe(1)−O(2)	2.137(2)
	Bond Angles [deg]		
N(1)−Fe(1)−N(3)	179.44(7)	N(2)−Fe(1)−O(2)	89.70(6)
N(1)−Fe(1)−N(2)	89.78(6)	N(4)−Fe(1)−O(2)	90.81(6)
N(3)−Fe(1)−N(2)	90.09(6)	N(1)−Fe(1)−O(1)	89.78(6)
N(1)−Fe(1)−N(4)	90.04(6)	N(3)−Fe(1)−O(1)	89.68(6)
N(3)−Fe(1)−N(4)	90.08(6)	N(2)−Fe(1)−O(1)	91.70(6)
N(2)−Fe(1)−N(4)	179.45(7)	N(4)−Fe(1)−O(1)	87.78(6)
N(1)−Fe(1)−O(2)	90.55(6)	O(2)−Fe(1)−O(1)	178.56(5)
N(3)−Fe(1)−O(2)	89.99(6)		

= tetrahydrofuran) that were suitable for X-ray analysis were obtained after two weeks from a saturated solution of the precursor in THF layered with *n*-hexane. Intensity data were collected using a STOE imaging-plate diffraction system with Mo Kα radiation. The structure was solved with direct methods using SHELXS-97,[27] and refinement was done against F^2 using SHELXL-97. All non-hydrogen atoms were refined with anisotropic displacement parameters. The hydrogen atoms were placed in ideal positions and refined isotropically using a riding model. There are three crystallographically independent THF molecules in the asymmetric unit. In two cases, three carbon atoms are disordered and were refined using a split model. The third THF molecule is disordered, and no appropriate split model could be found. Therefore, the data were corrected for disordered solvent using the "Squeeze" option in Platon. Selected crystallographic data are presented in Table 2. Selected bond lengths and angles are presented in Table 3. $[Fe(TPP)(thf)_2](BF_4)$ crystallizes in the triclinic space group $P\bar{1}$ with all of the atoms located in general positions. The iron atom is coordinated by the four porphyrin nitrogen atoms and an oxygen atom from each of the two thf ligands within a slightly distorted octahedron (Figure 1). The iron atom is located in the porphyrin ring plane (deviation from the mean plane: 0.0044 Å).

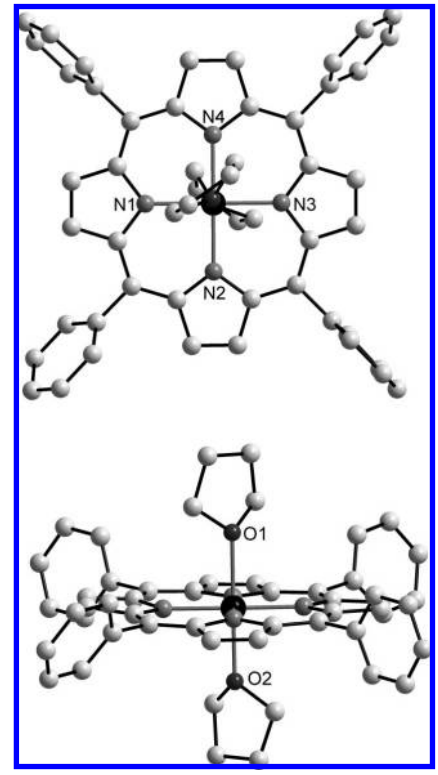

Figure 1. Top view (top) and side view (bottom) of the crystal structure of the important precursor $[Fe^{III}(TPP)(thf)_2](BF_4)$, shown with the atom-labeling scheme. The hydrogen atoms, disordered solvent molecules, and counteranion have been omitted for clarity.

UV−vis and IR Spectroscopy. Absorption spectra were recorded in CH_2Cl_2 solutions at room temperature using an Analytik Jena Specord S600 UV−vis spectrometer with glass fiber attachment. Middle-infrared (MIR) spectra were recorded on PerkinElmer Spectrum BX and GX FT-MIR spectrometers using KBr disks. The resolution was set to 2 cm^{-1}. In the far-infrared (FIR) region, a Nicolet DX version 4.56 spectrometer was employed. Spectra were recorded in CsI disks at a resolution of 2 cm^{-1}. All of the IR spectra were recorded at room temperature.

Nuclear Resonance Vibrational Spectroscopy (NRVS). NRVS data were obtained as described in ref 28 at beam line 3-ID-XOR of the Advanced Photon Source (APS) at Argonne National Laboratory. This beamline provides ~2.5 × 10^9 photons/s in a bandwith of ~1 meV (= 8 cm^{-1}) at 14.4125 keV in a 0.5 mm (vertical) × 0.5 mm (horizontal) spot. This is achieved using a water-cooled diamond double crystal monochromator with a 1.1 eV bandpass followed by a high-resolution monochromator consisting of two asymmetrically cut Si(4 0 0) and two asymmetrically cut Si(10 6 4) crystals.[29] Samples were loaded into 3 × 7 × 1 mm Lucite NRVS cells. Delayed nuclear fluorescence and Fe K fluorescence were detected using a single avalanche photodiode.[30] Spectra were recorded from −40 to 90 meV in steps of 0.25 meV. Each scan took ~60 min. All of the scans were added and normalized to the intensity of the incident beam. The final spectra represent averages of 6 scans. During data collection, the samples were maintained at cryogenic temperatures using a liquid helium cryostat. Because the temperature sensor is not in direct contact with the sample, the temperatures for individual scans are not exactly known. Since the anti-Stokes intensities of modes >100 cm^{-1} are negligible, the sample temperature was well below 50 K. Comparison of initial and final NRVS scans confirms the absence

(27) Sheldrick, G. M. *SHELXS-97 and SHELXL-97: Programs for the Solution and Refinement of Crystal Structures*; University of Göttingen: Göttingen, Germany, 1997.
(28) (a) Sturhahn, W. *J. Phys.: Condens. Matter* **2004**, *16*, S497–S530. (b) Petrenko, T.; DeBeer George, S.; Aliaga-Alcalde, N.; Bill, E.; Mienert, B.; Xiao, Y.; Guo, Y.; Sturhahn, W.; Cramer, S. P.; Wieghardt, K.; Neese, F. *J. Am. Chem. Soc.* **2007**, *129*, 11053–11060.
(29) Toellner, T. S. *Hyperfine Interact.* **2000**, *125*, 3–28.
(30) Baron, A. Q. R.; Kishimoto, S.; Morse, J.; Rigal, J.-M. *J. Synchrotron Radiat.* **2006**, *13*, 131–142.

Scheme 1

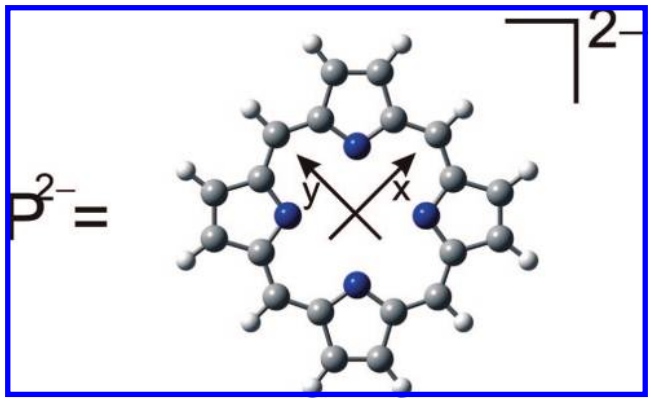

of spectroscopic changes due to radiation damage. MIR spectra of the samples were also recorded before and after exposure to the X-ray beam (Figures S4 and S5 in the Supporting Information), showing no degradation. NRVS raw data were converted to the vibrational density of states (VDOS) using the program Phoenix.[31,32]

DFT Calculations. The structures of the model systems [Fe(P)(MI)(NO)]$^+$ ($\tilde{\mathbf{1}}$, $S = 0$), [Fe(P)(MI)]$^+$ ($S = {}^1/_2, {}^5/_2$), and [Fe(P)(MI)] ($S = 0, 2$) were fully optimized at the BP86/TZVP level (i.e., using the BP86 functional and the TZVP basis set). These calculations used a simplified TPP ligand in which the four phenyl groups at the *meso* positions of the porphyrin ring were replaced by hydrogen. The resulting porphine ligand (P^{2-}) is shown in Scheme 1 along with the applied coordinate system. No imaginary frequencies were obtained for $\tilde{\mathbf{1}}$. In addition, B3LYP/LANL2DZ and B3LYP/LANL2DZ* geometry optimizations were performed on these models and the corresponding ferrous NO adduct [Fe(P)(MI)(NO)] ($S = {}^1/_2$) in order to investigate the method dependence of the complex formation energies. B3LYP/TZVP single-point calculations on the fully optimized B3LYP/LANL2DZ* structures were also employed. The LANL2DZ* basis set[21a] consists of the LANL2DZ basis set[33] plus polarization functions (from TZVP[34]) on all of the heavy atoms. The PES calculations employed B3LYP/LANL2DZ geometry optimizations in which the Fe−NO distances were fixed and all of the other internal coordinates were allowed to vary. The geometry of the Fe(III)−NO(radical) $S = 0$ state was also fully optimized and showed a linear Fe−N−O unit (vide infra). However, in the PES calculations for this state, the Fe−N−O angle was fixed at 170° for Fe−NO distances less than 2.64 Å because allowing this angle to optimize led to severe SCF convergence problems; in addition, the wave function frequently returned to the Fe(II)−NO$^+$ state. This problem was only observed at Fe−NO bond distances less than 2.64 Å and could be overcome by fixing the Fe−N−O angle at 170°. The error in the total energies induced this way is only ~0.2 kcal/mol (calculated for the fully optimized structure). B3LYP/TZVP single-point calculations were then performed on the B3LYP/LANL2DZ structures. Finally, to explore the effect of the phenyl substituents on the relative energies of the two singlet states, we fully optimized the structures of [Fe(TPP)(MI)(NO)]$^+$ (i.e., including the full TPP ligand) for both the Fe(II)−NO$^+$ and Fe(III)−NO(radical) $S = 0$ states using B3LYP/LANL2DZ. The obtained energy difference between these states is very similar to the value calculated with the porphine approximation. All of these methods were used as implemented in Gaussian 03.[35] Orbitals were plotted using GaussView.

Normal Coordinate Analysis. Normal-coordinate calculations were performed using the QCPE computer program 576 by M. R. Peterson and D. F. McIntosh. The calculations are based on a general valence force field; force constants are refined with a nonlinear simplex algorithm. The simplex optimization was used to refine only *selected* force constants according to our QCC-NCA scheme.[21b] In this case, a force field from DFT calculations is used as a starting point to generate initial force constants, and a subset of these are fit to reproduce the known experimental frequencies. Force constants were extracted from the Gaussian output using a modified version of the program Redong[36] (QCPE 628). We have now extended our QCC-NCA package to directly calculate NRVS VDOS intensities from the normal coordinate analysis results (vide infra). In order to simulate the vibrations of the Fe−N−O subunit of **1**, the force field calculated for model $\tilde{\mathbf{1}}$ was used for NCA. It should be noted that in this case, the two Fe−N−O linear bends show a calculated splitting of ~8 cm^{-1} that is not observed experimentally. We compensated for this in the NCA by allowing the two corresponding Fe−N−O bending force constants to have different values. The observed TPP-based vibrations in the NRVS spectra of **1** could not be simulated in the present NCA because of the use of porphine instead of TPP in the calculations. Corresponding large-scale calculations on the complete complex **1** including the full TPP ligand are currently underway to investigate the influence of the phenyl substituents of TPP on the vibrational properties of the complex. These studies will be the subject of a forthcoming paper.

Results and Analysis

A. Vibrational Spectroscopy and Electronic Structure of Fe(III)−Porphyrin NO Adducts in the Ground State. A.1. Vibrational Properties and Assignments. The MIR spectrum of [Fe(TPP)(MI)(NO)](BF$_4$) (**1**) is shown in Figure 2 together with the corresponding data for the $^{15}N^{18}O$-labeled analogue. The N−O stretching vibration ν(N−O) was identified as the band at 1896 cm^{-1} that shifts to 1816 cm^{-1} upon isotopic substitution. One other isotope-sensitive band is found at 588 cm^{-1}, which appears at 572 cm^{-1} in the $^{15}N^{18}O$ compound. It is not possible to tell a priori whether this feature belongs to the two (degenerate) Fe−N−O linear bends, δ_{lb}(Fe−N−O), or the Fe−NO stretch, ν(Fe−NO). In order to locate the other respective feature, resonance Raman measurements on frozen solutions of **1** at multiple excitation wavelengths were then conducted, but no unambiguous assignment could be obtained from these experiments. One general problem with resonance Raman spectroscopy on heme nitrosyls is the potential photodecomposition of the compounds by loss of either NO or the *trans* imidazole ligand. We therefore turned to nuclear resonance vibrational spectroscopy (NRVS), which is a method that (unlike resonance Raman) does not suffer from sample degradation. NRVS measures the inelastic scattering that is observed upon excitation of the ^{57}Fe nucleus at the 14.4125 keV nuclear resonance (Mössbauer) line.[28a,37] NRVS is ideal for the identification of metal−ligand stretching vibrations because NRVS intensities are proportional to the amount of iron motion in a normal mode.[31] Hence, metal−ligand stretching vibrations are very intense in NRVS, and this method has recently been successfully applied to ferrous heme nitrosyls and carbonyls.[25,38] Figure S3 in the Supporting Information shows the NRVS raw data for [^{57}Fe(TPP)(MI)(NO)](BF$_4$) (i.e., ^{57}Fe-substituted **1**) and the corresponding $^{15}N^{18}O$-labeled complex. The vibrational density of states (VDOS) calculated from these data is shown

(31) Sage, J. T.; Paxson, C.; Wyllie, G. R. A.; Sturhahn, W.; Durbin, S. M.; Champion, P. M.; Alp, E. E.; Scheidt, W. R. *J. Phys.: Condens. Matter* **2001**, *13*, 7707–7722.
(32) Sturhahn, W. *Hyperfine Interact.* **2000**, *125*, 149–172.
(33) (a) Hay, P. J.; Wadt, W. R. *J. Chem. Phys.* **1985**, *82*, 270–283. (b) Wadt, W. R.; Hay, P. J. *J. Chem. Phys.* **1985**, *82*, 284–298. (c) Hay, P. J.; Wadt, W. R. *J. Chem. Phys.* **1985**, *82*, 299–310.
(34) Schäfer, A.; Horn, H.; Ahlrichs, R. *J. Chem. Phys.* **1992**, *97*, 2571.
(35) Frisch, M. J.; et al. *Gaussian 03*; Gaussian, Inc.: Pittsburgh, PA, 2003.
(36) Allouche, A.; Pourcin, J. *Spectrochim. Acta* **1993**, *49A*, 571.
(37) Scheidt, W. R.; Durbin, S. M.; Sage, J. T. *J. Inorg. Biochem.* **2005**, *99*, 60–71.

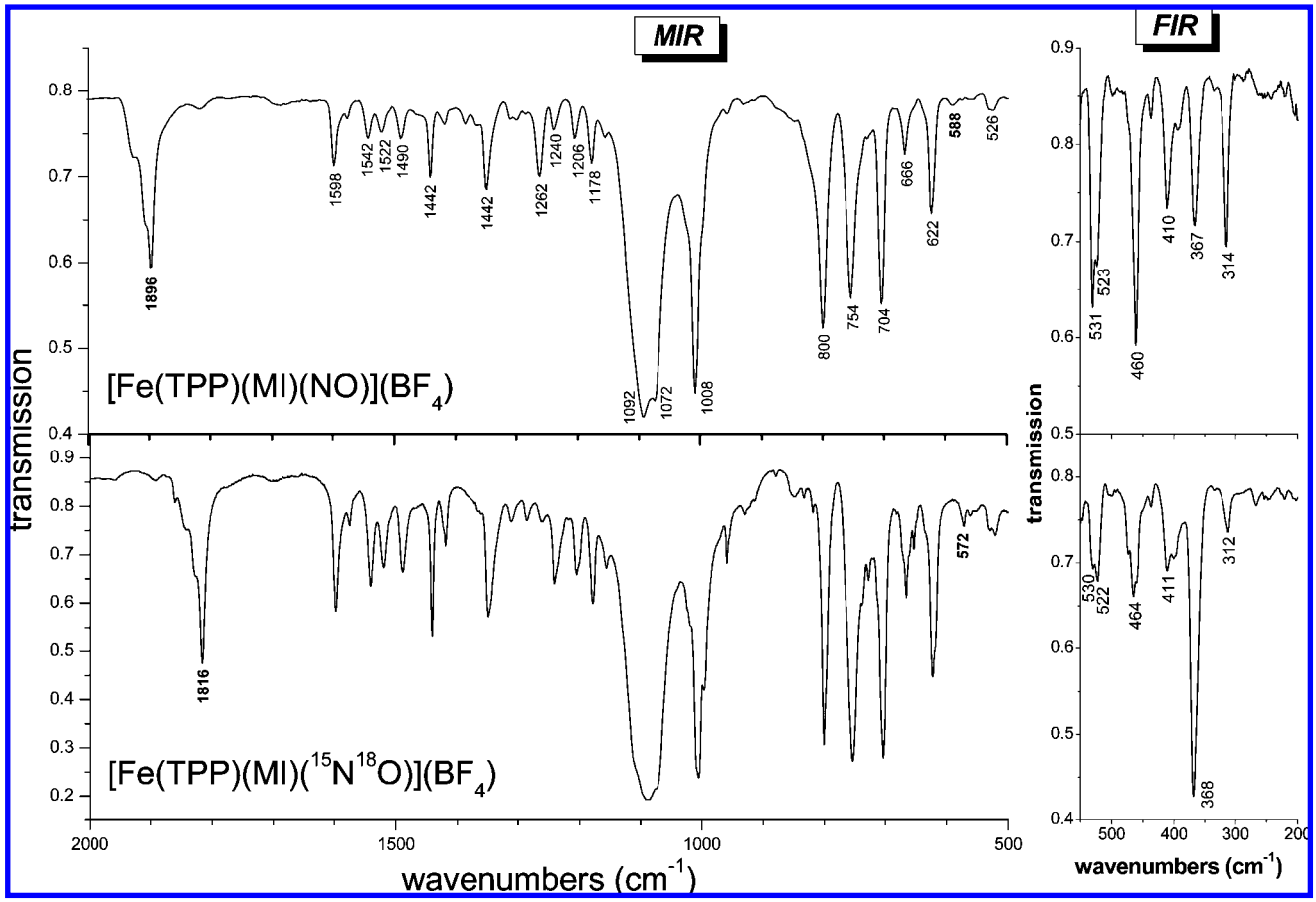

Figure 2. IR spectra of [Fe(TPP)(MI)(NO)](BF$_4$) (**1**) (top) and the corresponding $^{15}N^{18}O$-labeled complex (bottom): middle IR (left); far IR (right).

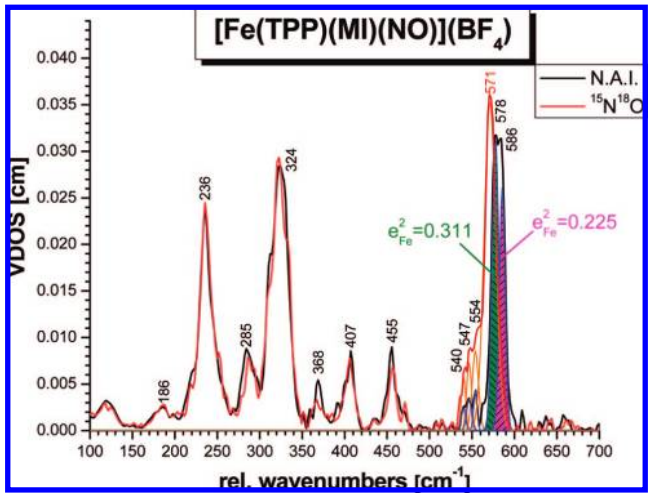

Figure 3. VDOS for [^{57}Fe(TPP)(MI)(NO)](BF$_4$) (with natural abundance isotopes (N.A.I.) NO) and for the corresponding $^{15}N^{18}O$-labeled complex, calculated from the NRVS raw data using Phoenix.[32] The N.A.I. NO (blue) and $^{15}N^{18}O$ (orange) fits of the isotope-sensitive feature near 580 cm^{-1} yielded total (combined) integrated intensities, $e_{Fe}{}^2$, of 0.536 (N.A.I.) and 0.545 ($^{15}N^{18}O$), showing that these two features are related.

in Figure 3. In the complex with unlabeled NO, two intense features that are close in energy (578 and 586 cm^{-1}) are observed. The mode at higher energy corresponds to the IR feature at 588 cm^{-1}, since a shift of 1−2 cm^{-1} to lower energy in the NRVS data can be attributed to the ^{57}Fe labeling in this case (this small energy difference is also below the resolution of the two methods). Importantly, the integrated VDOS intensity of a normal mode from NRVS, $e_{Fe}{}^2$, is proportional to the amount of iron motion in that mode.[31] As will be shown in section A.2, this quantity can be calculated in a straightforward fashion for a normal mode using NCA. In the case of the linear Fe−N−O unit in **1**, where no mixing between the Fe−NO stretch and the two (orthogonal) linear bends is possible, the amounts of iron motion in the stretch and the two bends are intrinsic properties of the Fe−N−O unit. Therefore, the relative NRVS intensities of these modes should be more or less constant[39] and are readily available from NCA. The NCA results presented below for **1**show that the Fe−NO stretch has a distinctively larger amount of iron motion and hence a larger NRVS intensity than the combined linear bends. This is a general feature of a linear Fe−X−O unit, and a similar intensity difference between ν(Fe−CO) and δ_{lb}(Fe−C−O) was observed in a recent NRVS study on [Fe(TPP)(MI)(CO)].[25]The theoretical NRVS intensity ratio for ν(Fe−NO) and δ_{lb}(Fe−N−O) from NCA was used to fit the spectrum in Figure 3.

(38) (a) Rai, B. K.; Durbin, S. M.; Prohofsky, E. W.; Sage, J. T.; Wyllie, G. R. A.; Scheidt, W. R.; Sturhahn, W.; Alp, E. E. *Biophys. J.* **2002**, *82*, 2951–2963. (b) Leu, B. M.; Zgierski, M. Z.; Wyllie, G. R. A.; Scheidt, W. R.; Sturhahn, W.; Alp, E. E.; Durbin, S. M.; Sage, J. T. *J. Am. Chem. Soc.* **2004**, *126*, 4211–4227. (c) Zeng, W.; Silvernail, N. J.; Wharton, D. C.; Georgiev, G. Y.; Leu, B. M.; Scheidt, W. R.; Zhao, J.; Sturhahn, W.; Alp, E. E.; Sage, J. T. *J. Am. Chem. Soc.* **2005**, *127*, 11200–11201. (d) Silvernail, N. J.; Barabanschikov, A.; Pavlik, J. W.; Noll, B. C.; Zhao, J.; Alp, E. E.; Sturhahn, W.; Sage, J. T.; Scheidt, W. R. *J. Am. Chem. Soc.* **2007**, *129*, 2200–2201. (e) Leu, B. M.; Silvernail, N. J.; Zgierski, M. Z.; Wyllie, G. R. A.; Ellison, M. K.; Scheidt, W. R.; Zhao, J.; Sturhahn, W.; Alp, E. E.; Sage, J. T. *Biophys. J.* **2007**, *92*, 3764–3783.

Table 4. Geometrical and Vibrational Properties of [Fe(P*)(L)(NO)] Complexes (L = MI, Py, etc., or Missing; P* = Tetraphenylporphyrin- or Octaethylporphyrin-Type Ligand)

	geometrical parameters					vibrational frequencies [cm^{-1}]		
molecule[a]	r(Fe−NO) [Å]	r(N−O) [Å]	∠(Fe−N−O) [deg]	r(Fe−L_{tr}) [Å]	r(Fe−N_P) [Å][b]	ν(N−O)	ν(Fe−NO)	δ(Fe−N−O)
			Fe^{III} Complexes					
[Fe(OEP)(NO)](ClO_4)[c,d]	1.644	1.112	177		1.994	1868	611	
[Fe(OEP)(MI)(NO)](ClO_4)[c]	1.646	1.135	177	1.988	2.003	1921		
[Fe(OEP)(Py)(NO)]Cl[e]							602	
[Fe(SP-14)(Py)(NO)]Cl[e]							603	
[Fe(TPP)(NO)](BF_4)						1853		
[Fe(TPP)(MI)(NO)](BF_4) (**1**)						1896	580[f]	587,[f] 588 (IR)
[Fe(TPP)(MI)($^{15}N^{18}O$)](BF_4)						1816	(∼569)[f]	(∼575),[f] 572 (IR)
[Fe(TPP)(NO)(NO_2)] (**2**)						1874		
[Fe(P)(MI)(NO)]$^+$ (**$\tilde{1}$**) (calcd)								
BP86/TZVP {Fe^{II}−NO^+}	1.644	1.147	180	2.018	2.022	1933	639	606/598
B3LYP/LANL2DZ {Fe^{II}−NO^+}	1.639	1.169	180	1.976	2.023	1908	657	613/601
B3LYP/LANL2DZ {Fe^{III}−NO(rad.)}	1.689	1.178	180	1.967	2.021	1841	430	570/523
[Fe(TPP)(MI)(NO)]$^+$ (calcd)								
B3LYP/LANL2DZ {Fe^{II}−NO^+}	1.644	1.173	173	1.976	2.013			
B3LYP/LANL2DZ {Fe^{III}−NO(rad.)}	1.673	1.180	179	1.975	2.010			
			Fe^{II} Complexes					
[Fe^{II}(TPP)(MI)(NO)] (**3**)[g]	1.750	1.182	138	2.173	2.008	1630	437	563(ip), 291(oop)
[Fe^{II}(P)(MI)(NO)] (calcd BP86/TZVP)[g]	1.734	1.186	140	2.179	2.022	1662	609	482(ip), 317(oop)

[a] MI = 1-methylimidazole; P = porphine ligand used in the calculations. [b] Values are averages over the four Fe−N_P bonds. [c] Data taken from ref 14a,b. [d] Chloroform solvate. [e] Data taken from ref 43. [f] NRVS data. Natural abundance isotopes energies at 580 and 587 cm^{-1} are estimated from the calculated ^{57}Fe shifts using NCA (experimental NRVS energies: 578 and 586 cm^{-1}, respectively). The energies in the $^{15}N^{18}O$ case can only be estimated because only one band, spectroscopically centered at 571 cm^{-1}, is observed (see text). [g] Data taken from ref 21b,e.

Table 5. Comparison of Experimental and QCC-NCA Vibrational Frequencies and of QCC-NCA and DFT-Calculated Force Constants for **1**

	vibrational frequencies [cm^{-1}]				force constants [mdyn/Å]		
	exptl		QCC-NCA			DFT-calculated[b]	
mode	N.A.I.[a]	$^{15}N^{18}O$	^{57}Fe	$^{15}N^{18}O$	QCC-NCA	Fe(II)−NO^+	LS Fe(III)−NO(rad.)
ν(N−O)[c]	1896	1816	1897	1815	15.178	15.62	13.72
ν(Fe−NO)	578[d]	(∼569)[d]	580	566	3.922	4.82	2.26
$δ_{lb}$(Fe−N−O)	586,[d] 588 (IR)	(∼575),[d] 572 (IR)	587	573	0.368/0.406 [e]	0.46/0.47	0.31/0.37

[a] N.A.I. = natural abundance isotopes. [b] Values for Fe(II)−NO^+ and LS Fe(III)−NO(radical) were calculated using BP86/TZVP and B3LYP/LANL2DZ, respectively (see DFT Calculations). [c] For free NO: ν(N−O) = 1876 cm^{-1}; N−O force constant = 15.49 mdyn/Å. For free NO^+: ν(N−O) = 2387 cm^{-1} in (NO^+)(BF_4^-); N−O force constant = 25.07 mdyn/Å.[46] [d] From NRVS using ^{57}Fe. Isotope shifts between N.A.I. iron and ^{57}Fe are in the range of 1−2 cm^{-1} and hence of the same magnitude as the experimental error in the NRVS frequencies (which is due to the required data fitting and the relatively low resolution of NRVS). In particular, the energies in the $^{15}N^{18}O$ case had to be estimated because only one band, spectroscopically centered at 571 cm^{-1}, was observed (see text). [e] DFT predicts a small splitting of the δ modes; the force constants were adjusted to ensure that the two components are isoenergetic.

Since the 586 and 578 cm^{-1} features in **1** are close in energy, their assignment is not straightforward. In the case of the ferric NO adduct of myoglobin, $δ_{lb}$(Fe−N−O) is found at somewhat higher energy than ν(Fe−NO),[40] but this trend is reversed in the case of the ferric cytochrome P450cam NO adduct[41] and also in six-coordinate (6C) ferrous heme carbonyls.[25] Therefore, a better way to assign the observed modes in **1** is to consider the fact that the 586 cm^{-1} feature is IR-active (observed at 588 cm^{-1}) whereas the mode at 578 cm^{-1} is not. Previous work on [$Ru(NH_3)_5$(NO)]X_3 (X = halide ion, etc.), a complex containing a linear Ru(II)−NO^+ unit similar to the Fe(II)−NO^+ unit in **1**, has shown that in this case the Ru−NO stretch is Raman active whereas the Ru−N−O linear bends are strongly IR active.[12b] Similar observations have been made for linear dinitrogen complexes (note that N_2 is isoelectronic to NO^+).[42] On this basis, the band at 588 cm^{-1} is assigned to the two Fe−N−O linear bends, $δ_{lb}$(Fe−N−O), and the feature at 578 cm^{-1} is then identified with ν(Fe−NO).

When $^{15}N^{18}O$ isotope labeling is used, ν(Fe−NO) and $δ_{lb}$(Fe−N−O) merge into the band centered at 571 cm^{-1}. This is evident from the fact that the total integrated VDOS intensity of this band (0.545) is comparable to the combined intensities of the 586 and 578 cm^{-1} features in the unlabeled complex (0.536). When the ratio of integrated intensities of the 586 and 578 cm^{-1} bands is kept constant (e_{Fe}^2[ν(Fe−NO)]/e_{Fe}^2[$δ_{lb}$(Fe−N−O)] ≈ 1.35), the 571 cm^{-1} feature in the $^{15}N^{18}O$-labeled complex can be approximately resolved into two features at 575 and 569 cm^{-1}, which correspond to $δ_{lb}$(Fe−N−O) and ν(Fe−NO), respectively. These assignments are listed in Tables 4 and 5. In summary, the NRVS measurements allow for the identification of ν(Fe−NO) and $δ_{lb}$(Fe−N−O) for the ferric heme NO model complex **1**. The

(39) This assumes that mode mixing of the Fe−NO stretch and of the linear Fe−N−O bends with porphyrin modes is reasonably small, which should in general be a good approximation for vibrations occurring in the 500−650 cm^{-1} range. Some mode mixing is of course observed, so small variations in the relative VDOS intensity of the stretch versus the bends are possible (see text).

(40) Benko, B.; Yu, N. T. *Proc. Natl. Acad. Sci. U.S.A.* **1983**, *80*, 7042–7046.

(41) Hu, S.; Kincaid, J. R. *J. Am. Chem. Soc.* **1991**, *113*, 2843–2850.

(42) Lehnert, N.; Tuczek, F. *Inorg. Chem.* **1999**, *38*, 1659–1670.

spectral assignments are further substantiated by simulation of the observed isotope shifts using NCA (vide infra).

The observed ν(N−O) frequency of 1896 cm^{-1} for **1** is in good agreement with the literature value of 1921 cm^{-1} obtained for [Fe(OEP)(MI)(NO)](ClO_4), as shown in Table 4. In proteins, 6C ferric heme NO adducts with trans histidine ligation also show N−O frequencies in the 1900 cm^{-1} region (Table 1). Interestingly, the Fe−NO stretch in these protein species (590−600 cm^{-1}) is slightly higher in energy than in **1**. In particular, the ferric NO adduct of rNp1 exhibits ν(N−O) at 1917 cm^{-1} and ν(Fe−NO) at 591 cm^{-1}. From solution studies of [Fe(OEP)(Py)(NO)]Cl and [Fe(SP-14)(Py)(NO)]Cl (SP-14 = strapped porphyrin) using resonance Raman spectroscopy (407 nm excitation), ν(Fe−NO) has been assigned to bands at 602 and 603 cm^{-1}, respectively.[43] The vibrational energies predicted by DFT (BP86/TZVP) for the model system [Fe(P)(MI)(NO)]$^+$ (**1̃**) are also in good agreement with experiment (Table 4). This is especially true for the N−O stretch, which is calculated at 1933 cm^{-1}. The calculated frequency of 639 cm^{-1} for the Fe−NO stretch shows a larger deviation. The fact that the Fe−NO bond strength and, correspondingly, the Fe−NO frequency are overestimated by DFT is not uncommon[16] and was also observed for ferrous heme nitrosyls.[21b]

As mentioned in the Introduction, detailed vibrational studies of ferric heme NO model complexes are rare. This is most likely due to the fact that these complexes are unstable and tend to decompose by either loss of NO or reaction with O_2 to form the nitro-nitrosyl adduct [Fe(porphyrin)(NO)(NO_2)]. In order to ensure that compound **1** does not correspond to [Fe(TPP)(NO)(NO_2)] (**2**), we prepared this complex and investigated its vibrational properties. Figure S1 in the Supporting Information shows a comparison of the IR spectra of **1** and **2**, which are clearly different. In the case of **2**, ν(N−O) is located at 1874 cm^{-1}. The N−O stretching frequencies of the coordinated nitrite ligand are observed as characteristic bands at 1461 cm^{-1} for $\nu_{as}(NO_2)$ and 1299 cm^{-1} for $\nu_s(NO_2)$ (assignments from ref 44). These shift to 1401 and 1238 cm^{-1}, respectively, when $^{15}N^{18}O$ is used (Figure S2 in the Supporting Information), in agreement with this assignment. Importantly, both bands are missing in the spectrum of **1** (Figure S1), confirming that complex **1** is not the nitro-nitrosyl complex.

A.2. Quantum Chemistry Centered Normal Coordinate Analysis (QCC-NCA). A normal-coordinate analysis was carried out in order to substantiate the vibrational assignments for **1** and obtain experimental force constants for the Fe−NO and N−O bonds. An initial force field was calculated for the model complex [Fe(P)(MI)(NO)]$^+$ (**1̃**), and selected force constants were then refined in the fitting procedure according to the QCC-NCA approach.[21b] Masses of 77 were substituted for the *meso* hydrogen atoms of P^{2-} in the model system to better represent the *meso* phenyl groups of **1**. As shown in Table 5, excellent agreement between the vibrational frequencies from the NCA treatment and the experimental data is obtained. The corresponding force constants of the N−O and Fe−NO bonds are determined to be 15.18 and 3.92 mdyn/Å, respectively. Since the Fe−NO stretch and the two linear bends do not mix in the linear Fe−N−O geometry of **1**, the integrated VDOS intensity, e_{Fe}^2, and thus the ratio of the iron displacements r_{Fe}^2 of the Fe−NO stretch and the two Fe−N−O linear bends are intrinsic properties of the linear Fe−N−O unit that can be estimated from NCA. The integrated NRVS VDOS intensity e_{Fe}^2 for a given normal mode is readily obtained from NCA using the atomic-displacement matrix together with the following equation:[38b]

$$e_{Fe}^2 = \frac{m_{Fe} r_{Fe}^2}{\sum_i m_i r_i^2}$$

where the sum over i runs over all atoms of the molecule and r_i is the absolute length of the mass-weighted atomic-displacement vector for atom i from NCA. For **1**, the ratio of the e_{Fe}^2 values for the stretch and the linear bends can be estimated as follows:

$$\frac{e_{Fe}^2[\nu(\text{Fe−NO})]}{e_{Fe}^2[\delta_{lb}(\text{Fe−N−O})]} = \frac{0.436}{0.173 + 0.149} = \frac{0.436}{0.322} \approx 1.35$$

This value was used as a constraint in the fitting of the NRVS data for **1**. This is necessary because the Fe−NO stretch and the Fe−N−O linear bends are not resolved as individual peaks in the data, and hence, the fit is otherwise ambiguous. Interestingly, the absolute values of e_{Fe}^2 for both the stretch and the linear bends are overestimated in the NCA by ~30%. This is due to the neglect of the phenyl rings of TPP in the NCA (and in the DFT calculations), which reduces the effective mass of the porphyrin ligand, and also to mode mixing of ν(Fe−NO) and δ_{lb}(Fe−N−O) with porphyrin modes. A further investigation of this point is the subject of an ongoing study.

The observed N−O stretching frequency and the corresponding force constant are in good agreement with the generally accepted Fe(II)−NO^+ description of the ferric heme NO adducts (vide infra).[8a,11] The large Fe−NO force constant of 3.92 mdyn/Å is consistent with the presence of two strong π backbonds between the two occupied d_π orbitals of iron and the unoccupied π^* orbitals of NO^+. In comparison, force constants of 15.4 and 5.0 mdyn/Å have been obtained for the N−O and Ru−NO bonds, respectively, in the Ru(II)−NO^+ moiety of [$Ru(NH_3)_5$(NO)]Br_3, which exhibits a similar bonding situation.[12b] For the ferric NO adduct of Np1, N−O and Fe−NO force constants of 15.11 and 4.09 mdyn/Å, respectively, have been estimated using a simple eight-atom model for the NCA.[45] Nevertheless, these results show that **1** serves as an excellent model system for ferric Np1−NO.

A.3. Electronic Structure of [Fe(P)(MI)(NO)]$^+$ (1̃). The electronic structure of the ferric six-coordinate (6C) complex [Fe(TPP)(MI)(NO)]$^+$ (i.e., the cation of **1**) was analyzed in this study using the model complex **1̃**. Geometry optimization of this system was performed using BP86/TZVP and B3LYP/LANL2DZ. As shown in Table 4, both methods give very good agreement with the crystal structure of the 6C complex [Fe(OEP)(MI)(NO)](ClO_4).[14a] In particular, the very short Fe−NO bond (<1.65 Å) and the linear Fe−N−O unit are reproduced by DFT. For the further analysis of the electronic structure of **1**, the BP86/TZVP-optimized model **1̃** shown in Figure 4 is used for consistency with earlier work on ferrous heme NO adducts.[21] In the following evaluation of the molecular orbital (MO) diagram of **1̃**, the coordinate system shown in Scheme 1 is employed.

(43) Lipscomb, L. A.; Lee, B.-A.; Yu, N.-T. *Inorg. Chem.* **1993**, *32*, 281–286.
(44) Novozhilova, I. V.; Coppens, P.; Lee, J.; Richter-Addo, G. B.; Bagley, K. A. *J. Am. Chem. Soc.* **2006**, *128*, 2093–2104.
(45) Maes, E. M.; Walker, F. A.; Monfort, W. R.; Czernuszewicz, R. S. *J. Am. Chem. Soc.* **2001**, *123*, 11664–11672.
(46) Fadini, A.; Schnepel, F.-M. *Schwingungsspektroskopie*; Thieme Verlag: Stuttgart, Germany, 1985.

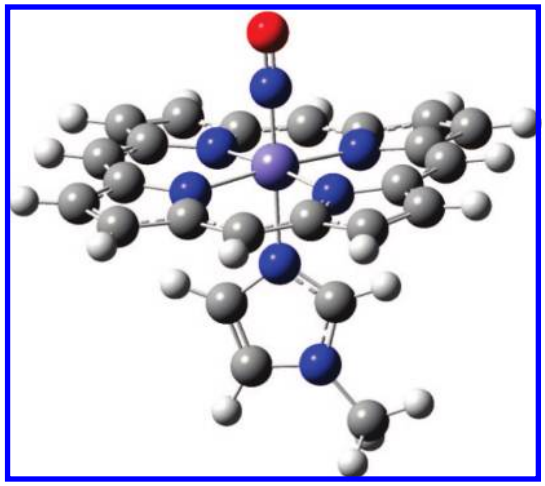

Figure 4. Fully optimized structure of $[Fe(P)(MI)(NO)]^+$ ($\tilde{\mathbf{1}}$, P = porphine, MI = 1-methylimidazole) obtained using BP86/TZVP. Important structural parameters are given in Table 4.

Figure 5 shows the MO diagram obtained for complex $\tilde{\mathbf{1}}$. Contour plots of important MOs are presented in Figure 6. As evidenced by the N−O stretching frequency of ~1900 cm^{-1} (vide supra) and the linear Fe−N−O unit, and in agreement with the literature[8a,11] and recent DFT results,[16] the electronic structure of complex **1** can in general be classified as Fe(II)−NO^+. Since iron is in the +2 oxidation state and low-spin in these compounds (as evident from magnetic Mössbauer measurements), it has a $[d_{xz}d_{yz}d_{x^2-y^2}]^6 \approx [t_2]^6$ electron configuration. Both π^* orbitals of the NO^+ ligand (isoelectronic to N_2) are empty and hence undergo π back-bonding interactions with the d_{xz} and d_{yz} orbitals of the metal in the applied coordinate system. The corresponding bonding combinations, d_{xz}_π_x^* and d_{yz}_π_y^* (see Figure 5 for notation), are delocalized over several MOs (see MOs <111> and <110> in Table 6). Hence, the strength of this back-bond is better estimated from the corresponding antibonding combinations, π_x^*_d_{xz} <123> and π_y^*_d_{yz} <124>, which are the LUMOs of complex $\tilde{\mathbf{1}}$. Both have ~68% π^* and ~27% d orbital character, which corresponds to a very strong π back-bonding interaction. Contour plots of these orbitals are shown in Figure 6. The third t_2-type d orbital of iron, $d_{x^2-y^2}$ <118>, is practically nonbonding (see Table 6). In summary, the calculated orbital coefficients are also in agreement with the Fe(II)−NO^+ description. However, the obtained N−O force constant of 15.18 mdyn/Å is markedly lower than that of free NO^+ (25.1 mdyn/Å) and is actually very close to that of free NO.[46] This is in agreement with the existence of two very strong Fe−NO π back-bonds, which lead to the transfer of a significant amount of electron density from the d_{xz} and d_{yz} orbitals of Fe to the π^* orbitals of NO. The total donation corresponds to approximately one electron. In addition, there is a very weak σ interaction between σ_{nb} of NO^+ and d_{z^2} of Fe. The corresponding bonding combination, σ_{nb}_d_{z^2} <66>, has 51% σ_{nb} and only 4% d_{z^2} contributions.

A.4. The Bending of the Fe−N−O Unit. Besides the two strong Fe−NO π bonds in ferric heme complexes, additional contributions to the Fe−NO bond have been proposed in recent DFT studies and related to a bending of the Fe−N−O unit.[16] In 5C ferric heme NO adducts, a direct correlation of the Fe−NO and N−O stretching frequencies was observed in DFT calculations upon core substitution of the porphyrin macrocycle.[16a] This has been related to a small admixture of a fully Fe−N−O σ antibonding orbital (d_{z^2}_σ^* in our notation) into the occupied porphyrin A_{2u} <81> HOMO. This mechanism leads to the partial population of an Fe−N−O antibonding orbital, which explains the observed trend in the DFT calculations: a larger population of this orbital leads to smaller values of both ν(N−O) and ν(Fe−NO) and vice versa. In addition, this is accompanied by a bending of the Fe−N−O unit. Experimentally, bending of the Fe−N−O unit is observed for ferric heme nitrosyls with axial thiolate coordination. Interestingly, in a recent study, the same mechanism (i.e., admixture of this d_{z^2}_σ^* orbital into the occupied porphyrin A_{2u} <81> HOMO) was shown to be responsible for the direct correlation of the ν(Fe−NO) and ν(N−O) frequencies in these systems and the observed Fe−N−O bending.[19] In this case, this is mediated by a *trans* effect of the thiolate. This interesting electronic effect is further substantiated by a comparison with complex **1** investigated here: in this case,

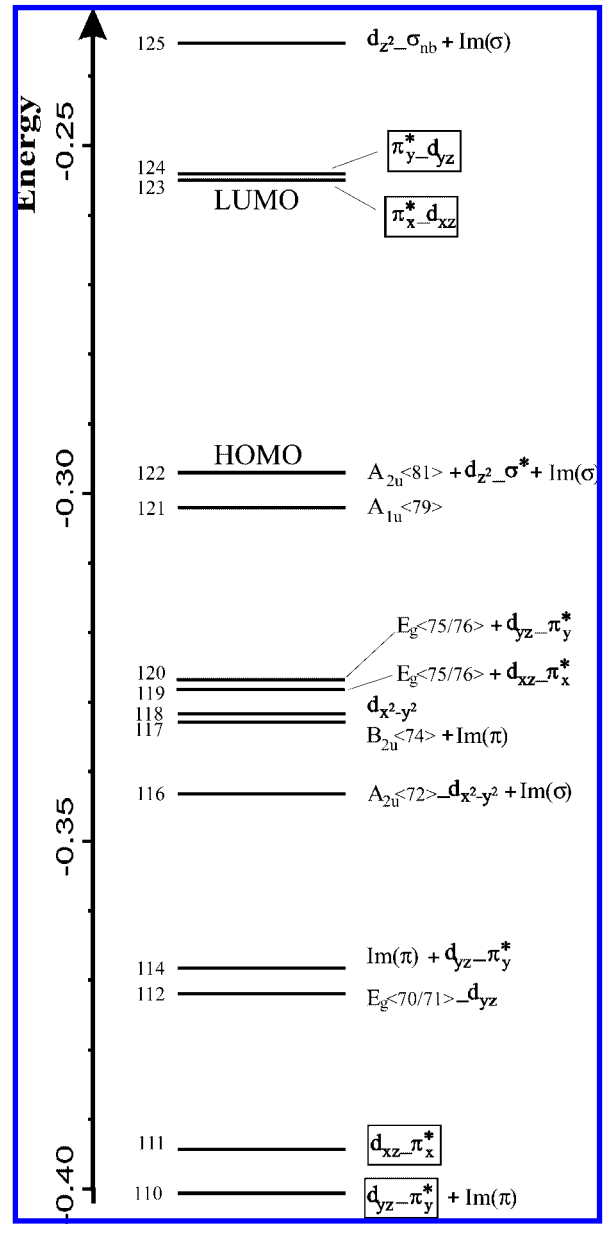

Figure 5. MO diagram of $[Fe(P)(MI)(NO)]^+$ ($\tilde{\mathbf{1}}$) calculated using BP86/TZVP. The applied coordinate system is shown in Scheme 1. The labels A_{1u}, A_{2u}, B_{2u}, and E_g refer to porphine orbitals (shown in Figure S7 in the Supporting Information).[21b] The notation "A_B" indicates that orbitals A and B interact, with A making the larger contribution to the resulting MO.

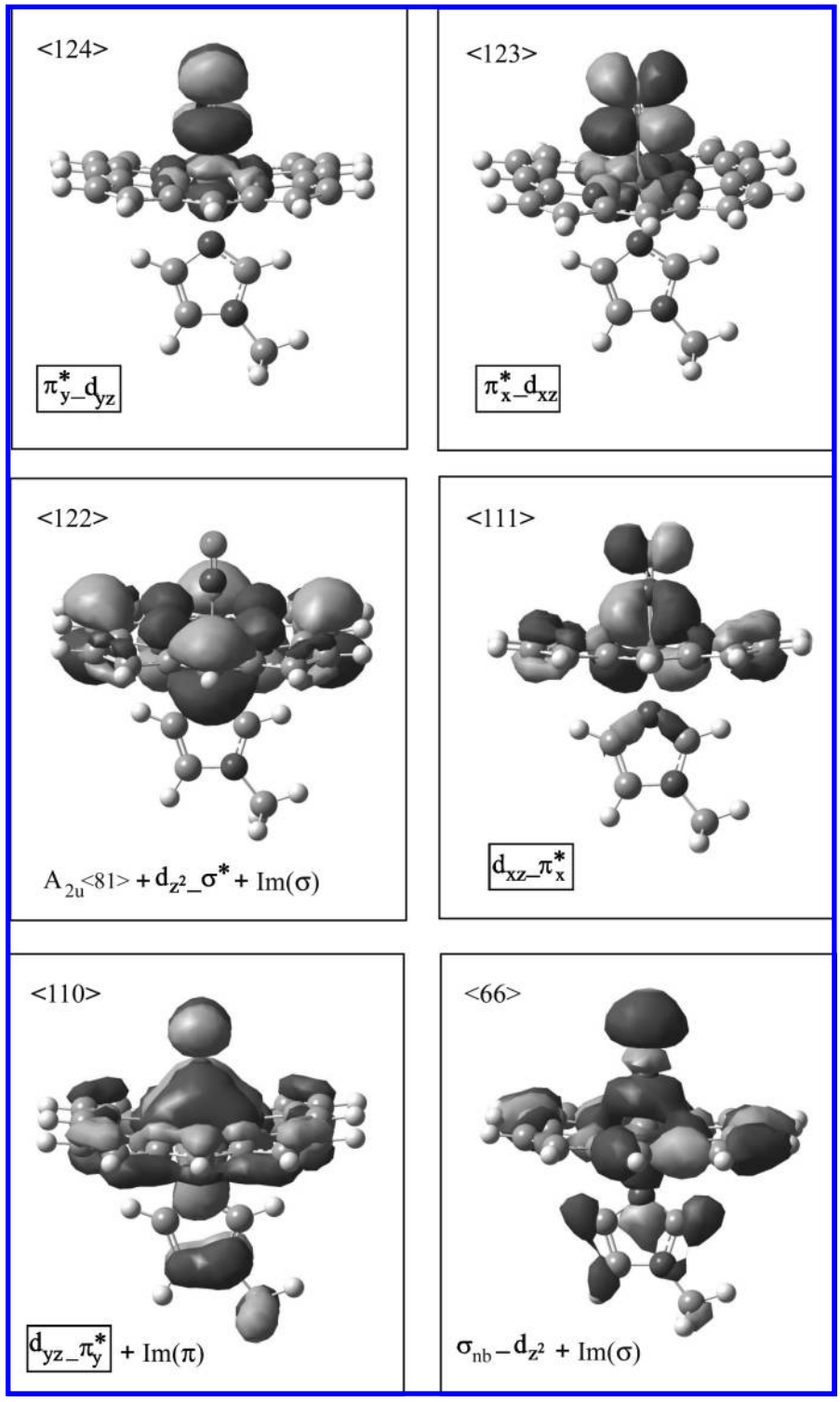

Figure 6. Contour plots of important MOs of $[Fe(P)(MI)(NO)]^+$ ($\tilde{\mathbf{1}}$) calculated using BP86/TZVP. The labels are explained in Figure 5 and Table 6.

the admixture of the Fe−N−O antibonding d_{z^2}_σ^* orbital into the A_{2u} <81> HOMO of the complex (see MO <122> of $\tilde{\mathbf{1}}$) is very small (only 1% d_{z^2} and 0.3% σ^* contributions), which is negligible with respect to the total Fe−NO bond strength (see Table 6). Correspondingly, this complex has a linear Fe−N−O unit and larger ν(Fe−NO) and ν(N−O) frequencies than the complexes with axial thiolate coordination. Contrary to these findings, it has also been proposed that the nature of the N−O antibonding orbital admixed into the porphyrin A_{2u} <81> HOMO changes to a π^*-type orbital (antibonding combination of d_π and π^*) in the 6C case.[16b] We found no evidence for this in our studies on the 6C complex **1**, so this does not seem to be a general property of 6C ferric heme nitrosyls.

B. Nitric Oxide Binding to Ferrous and Ferric Porphyrin Complexes. B.1. Energetic Considerations and Method Calibration. The stabilities of the ferrous and ferric NO complexes are determined from the following complex formation reactions using DFT calculations:

$$\text{HS-[Fe(P)(MI)]}^{n+} + \text{NO} \rightarrow \text{LS-[Fe(P)(MI)(NO)]}^{n+} \quad (n = 0, 1) \tag{1}$$

The calculated complex formation energies for both low-spin (LS) and high-spin (HS) reactants $[Fe(P)(MI)]^{n+}$ are listed in Table 7. From experiment, it is known that both ferrous and ferric five-coordinate (5C) hemes with axial imidazoles are high-spin.[47−49] As will be shown in the following analysis, the prediction of the correct ground state for the reactant turned out to be a major challenge for DFT. Importantly, the calculated reaction energies, $\Delta\varepsilon$, exhibit a large degree of method dependence, as shown in Table 7. Using BP86/TZVP gave unrealistically large energies ($|\Delta\varepsilon| > 30$ kcal/mol), and the 5C reactants are predicted to be low-spin for both ferrous and ferric heme. Hence, as has been noted before, total energy calculations with gradient-corrected functionals are problematic.[50] Therefore, we instead focused on using the B3LYP functional. Using B3LYP/LANL2DZ* calculations on the fully optimized structures from BP86/TZVP leads to much more realistic reaction energies. For the ferrous case, eq 1 is exothermic, with $\Delta\varepsilon = -16.7$ kcal/mol. In this case as well as in all of the other B3LYP calculations, the correct high-spin ground state for the ferrous reactant is predicted. In the ferric case, this approach leads to degenerate HS and LS states for $[Fe(P)(MI)]^{+}$ and $\Delta\varepsilon \approx -12.5$ kcal/mol. In order to further improve on these numbers, we next applied full geometry optimizations using B3LYP/LANL2DZ*. This way, reaction energies of −16 kcal/mol (ferrous) and roughly −13 kcal/mol (ferric) were obtained; in the latter case, the wrong ground state for the reactant is still predicted. Finally, we used B3LYP/TZVP single-point calculations on the B3LYP/LANL2DZ* structures. In this case, a complex formation energy of −11.4 kcal/mol is obtained for the ferrous complex. Importantly, this method finally predicted the correct HS ground state for ferric $[Fe(P)(MI)]^{+}$, with a calculated HS/LS energy difference of 5.6 kcal/mol. Because of this stabilization of the HS state of the reactant, the magnitude of the reaction energy from eq 1 decreased dramatically, and a $\Delta\varepsilon$ value of only −3.9 kcal/mol was obtained. In summary, these calculations show that the formation of nitrosyl complexes is energetically more favorable for ferrous compared to ferric hemes by ∼7.5 kcal/mol. This number is equivalent to a factor of 3×10^5 difference in the NO binding constant. This is in excellent agreement with the experimentally determined trend in dissociation rate constants: for ferric hemes, dissociation rate constants range from 0.65 to 40 s^{-1}, leading to a relatively small binding constant for NO ($K_{eq} = 10^3-10^5$ M^{-1}). In contrast, for Fe(II) systems, the dissociation rate constants are on the order of 10^{-4} s^{-1}, leading to very large binding constants for NO ($K_{eq} = 10^{11}-10^{12}$ M^{-1}).[51] *The calculated complex formation energies therefore show that the Fe−NO bond is thermodynamically stronger in*

Table 6. Charge Contributions of Important MOs of $[Fe(P)(MI)(NO)]^{+}$ ($\tilde{\mathbf{1}}$) Calculated Using BP86/TZVP

			Fe	N		O			
MO no.	label	energy [hartree]	d	s	p	s	p	N_{MI} (s + p)	∑MI
<125>	d_{z^2}_σ_{nb} + Im(σ)	−0.23526	56	4	3	1	2	9	11
<124>	π_y*_d_{yz}	−0.25401	27	0	42	0	26	0	1
<123>	π_x*_d_{xz} (LUMO)	−0.25465	27	0	42	0	26	0	0
<122>	A_{2u}<81> + d_{z^2}_σ* (HOMO)	−0.29701	1	0.2	0.1	0	0	2	2
<121>	A_{1u}<79>	−0.30203	0	0	0	0	0	0	0
<120>	E_g<75/76> + d_{yz}_π_y*	−0.32744	10	0	2	0	2	0.5	1
<119>	E_g<75/76> + d_{xz}_π_x*	−0.32773	10	0	3	0	2	0	0
<118>	$d_{x^2-y^2}$	−0.33166	86	0	0	0	0	0	0
<117>	B_{2u}<74> + Im(π)	−0.33288	0	0.3	0.2	0	0	1	41
<116>	A_{2u}<72> + $d_{x^2-y^2}$	−0.34318	6	0.3	0.2	0	0	2	2
<114>	Im(π) + d_{yz}_π_y*	−0.36820	14	0	2	0	4	18	52
<112>	E_g<70/71>	−0.37193	2	0	0	0	0	5	13
<111>	d_{xz}_π_x*	−0.39427	55	0	6	0	13	1	1
<110>	d_{yz}_π_y* + Im(π)	−0.40249	36	0	5	0	13	5	14
<109>	E_u<77/78> + π_x*	−0.40746	1	0	1	0	4	0	0
<108>	B_{1u}	−0.41055	0	0	0	0	0	0	0
<107>	E_u<77/78> + Im(π)_d_{yz}	−0.41102	4	0	0	0	0	5	21
<106>	B_{1g}<80>_d_{xy}	−0.43033	19	0	0	0	0	0	0
<102>	Im(σ)_d_{z^2} + σ_{nb}	−0.44589	13	1	1	0	1	36	67
<73>	π_x^b	−0.61229	2	0	41	0	47	0	0
<72>	π_y^b	−0.61271	3	0	43	0	48	0	0
<66>	σ_{nb}_d_{z^2} + Im(σ)	−0.63694	4	2	14	9	26	2	7

Table 7. Reaction Energies for $[Fe(P)(MI)]^{n+}$ + NO → $[Fe(P)(MI)(NO)]^{n+}$ at 298.15 K

		Δε(BP86) [kcal/mol]		Δε(B3LYP) [kcal/mol][b]	
complex	method	HS educt	LS educt	HS educt	LS educt
$[Fe^{II}(P)(MI)]$ + NO	BP86/TZVP full opt.	−44.1	−37.9	**−16.7**[a]	−22.3[a]
$[Fe^{III}(P)(MI)]^{+}$ + NO		−53.4	−41.2	−12.6[a]	**−12.3**[a]
$[Fe^{II}(P)(MI)]$ + NO	B3LYP/LANL2DZ full opt.	Structure of NO adduct incorrectly described			
$[Fe^{III}(P)(MI)]^{+}$ + NO				**−8.9**	−9.2
$[Fe^{II}(P)(MI)]$ + NO	B3LYP/LANL2DZ* full opt.			**−16.1**	−21.7
$[Fe^{III}(P)(MI)]^{+}$ + NO				−13.3	**−12.8**
$[Fe^{II}(P)(MI)]$ + NO	B3LYP/LANL2DZ*//B3LYP/TZVP			**−11.4**	−18.8
$[Fe^{III}(P)(MI)]^{+}$ + NO				**−3.9**	−9.5

[a] From single-point B3LYP/LANL2DZ* calculations on the fully optimized BP86/TZVP structures. [b] Bold numbers indicate the lower complex formation energy.

ferrous than in ferric heme NO adducts. In contrast, the Fe−NO force constant is distinctively *smaller* in ferrous heme NO adducts and has been determined to have the value 2.38 mdyn/Å in the directly related six-coordinate complex [Fe^{II}(TPP)(MI)(NO)] (**3**).[21e] This again raises the question of why the Fe−NO force constant is so much larger in the ferric case and how this relates to the complex stabilities and thermodynamic Fe−NO bond strengths.

B.2. Potential Energy Surface (PES) Calculations for the Interaction of NO with Ferric Heme. In order to obtain detailed insight into the mechanism of NO binding to five-coordinate (5C) ferric heme, we next performed PES calculations using model system $\tilde{\mathbf{1}}$ on (a) the closed-shell Fe(II)−NO^+ electronic state and (b) the Fe(III)−NO(radical) electronic state, where the unpaired electrons of Fe(III) and NO are antiferromagnetically coupled. Since the 5C reactant $[Fe(P)(MI)]^+$ can either be high-spin or low-spin, we considered both of these spin states in the calculations; therefore, in case (b), the total spin is either $S = 0$ [low-spin Fe(III)] or $S = 2$ [high-spin Fe(III)]. Geometry optimizations were performed on these three different electronic structures, varying the Fe−NO distance in a systematic way between 1.5 and 5 Å. Because this endeavor requires a very large number of calculations, we employed the B3LYP/LANL2DZ method for these partial optimizations, since this method generates a fully optimized structure for model system $\tilde{\mathbf{1}}$ that compares well with experiment and the BP86/TZVP structure (see Table 4). Figure S6 in the Supporting Information shows the PES obtained from these calculations. Importantly, B3LYP/LANL2DZ predicts that the Fe(III)−NO(radical) ($S = 0$) state is in fact the ground state of the complex, being 1.0 kcal/mol lower in energy than the Fe(II)−NO^+ state. Since this is not in agreement with experiment, we then performed B3LYP/TZVP single-point calculations on the B3LYP/LANL2DZ structures for the two $S = 0$ states, because this method has been shown to give better energies, as described in section B.1. The $S = 2$ surface was not recalculated but instead was shifted in energy to reproduce the calculated NO dissociation energy of ∼4 kcal/mol obtained from the B3LYP/TZVP treatment (Table 7), which is in better agreement with experiment. Figure 7 shows the three PES obtained this way.

In order to investigate whether the porphine approximation has a significant effect on the calculated energies of the $S = 0$ states, we also fully optimized the structure of [Fe(TPP)(MI)(NO)]$^+$ without any simplification (i.e., applying the complete TPP ligand). Importantly, the observed energy difference between the Fe(III)−NO(radical) $S = 0$ state and the Fe(II)−NO^+ state in this case is 1.3 kcal/mol, which compares well with the value of 1.0 kcal/mol obtained with the porphine approximation. Structural parameters are listed in Table 4. As observed in previous work,[21b] the phenyl substituents have only a small effect on the properties of the central Fe−N−O unit in heme nitrosyls.

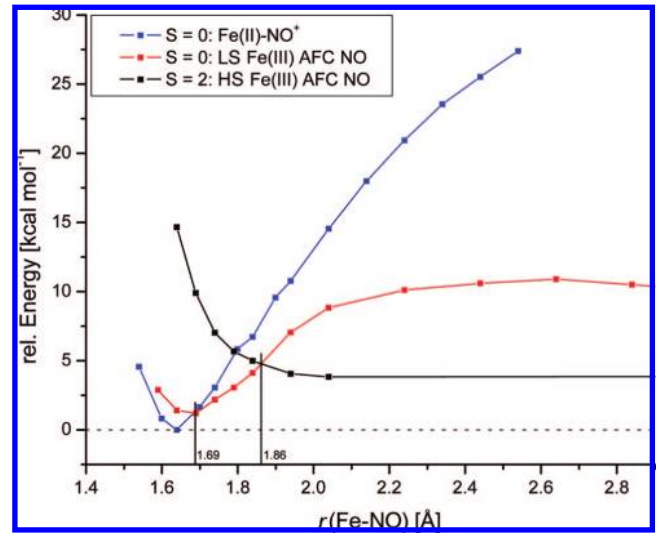

Figure 7. Potential energy surfaces for (a) closed-shell Fe(II)−NO^+ (blue), (b) LS Fe(III) antiferromagnetically coupled (AFC) to NO (open shell $S = 0$, red), and (c) HS Fe(III) AFC to NO ($S = 2$, black). Surfaces (a) and (b) were obtained using single-point B3LYP/TZVP calculations on the B3LYP/LANL2DZ structures (see Figure S6 in the Supporting Information). Surface (c) was obtained by shifting the corresponding B3LYP/LANL2DZ surface to lower energy to reproduce the calculated NO dissociation energy of 3.9 kcal/mol obtained with B3LYP/TZVP (Table 7). All of the calculations were performed using model complex $[Fe(P)(MI)(NO)]^+$ ($\tilde{\mathbf{1}}$).

As shown in Figure 7, the B3LYP/TZVP calculations predict the Fe(II)−NO^+ state to have the lowest energy, in agreement with experiment (vide supra). The corresponding PES for this state (shown in blue in Figure 7) is unusually steep for a metal−ligand bond, which is a result of the fact that a dissociation of the complex into Fe(II) and NO^+ is energetically very unfavorable. The equilibrium Fe−NO distance for this state is predicted to be <1.65 Å (Table 4), which is in excellent agreement with experiment (vide supra). The Fe−N−O unit in this state is linear. The PES for the $S = 0$ state in which low-spin Fe(III) is antiferromagnetically coupled to NO (the LS Fe(III)−NO(radical) state) is shown in red in Figure 7. To our great surprise, this state is energetically very close to the Fe(II)−NO^+ ground state (predicted to be ∼1.0 kcal/mol higher in energy). In this case, a stable minimum is obtained. Calculated spin densities are +0.84 on Fe and −0.73 on NO, which resembles the antiferromagnetic coupling between LS Fe(III) and NO. The two unpaired electrons are roughly located in the d_{yz} and π_y^* orbitals (see below). Therefore, because of the small energetic separation between the two $S = 0$ states, the Fe(II)−NO^+ PES crosses the LS Fe(III)−NO(radical) surface at an elongation of the Fe−NO bond of only ∼0.05 Å from the equilibrium distance. In addition, *the crossing from the Fe(II)−NO^+ state to the LS Fe(III)−NO(radical) state does not produce a bending of the Fe−N−O unit*: full geometry optimization of the LS Fe(III)−NO(radical) state leads to an Fe−NO bond length of 1.69 Å and a linear Fe−N−O unit. The electronic structure of this state is illustrated in Scheme 2. In this case, a strong polarization of the Fe−NO back-bond is observed, where the α-spin interaction almost disappears. MO coefficients for the corresponding antibonding combinations

(47) Walker, F. A.; Simonis, U. In *Encyclopedia of Inorganic Chemistry*, 2nd ed; King, R. B., Ed.; Wiley: Chichester, U.K., 2005; Vol. IV, pp 2390−2521.
(48) Scheidt, W. R.; Geiger, D. K.; Lee, Y. J.; Reed, C. A.; Lang, G. *J. Am. Chem. Soc.* **1985**, *107*, 5693–5699.
(49) Momenteau, M.; Loock, B.; Tetreau, C.; Lavalette, D.; Croisy, A.; Schaeffer, C.; Huel, C.; Lhoste, J.-M. *J. Chem. Soc., Perkin Trans. 2* **1987**, 249–257.
(50) (a) Ghosh, A.; Persson, B. J.; Taylor, P. R. *J. Biol. Inorg. Chem.* **2003**, *8*, 507–511. (b) Ghosh, A.; Vangberg, T.; Gonzalez, E.; Taylor, P. *J. Porphyrins Phthalocyanines* **2001**, *5*, 345–356. (c) Swart, M.; Groenhof, A. R.; Ehlers, A. W.; Lammertsma, K. *J. Phys. Chem. A.* **2004**, *108*, 5479–5483. (d) Chang, C. H.; Boone, A. J.; Bartlett, R. J.; Richards, N. G. J. *Inorg. Chem.* **2004**, *43*, 458–472.
(51) (a) Antonini, E.; Brunori, M.; Wyman, J.; Noble, R. W. *J. Biol. Chem.* **1966**, *241*, 3236–3238. (b) Traylor, T. G.; Sharma, V. S. *Biochemistry* **1992**, *31*, 2847–2849. (c) Sharma, V. S.; Traylor, T. G.; Gardiner, R.; Mizukami, H. *Biochemistry* **1987**, *26*, 3837–3843. (d) Hoshino, M.; Ozawa, K.; Seki, H.; Ford, P. C. *J. Am. Chem. Soc.* **1993**, *115*, 9568–9575.

Scheme 2

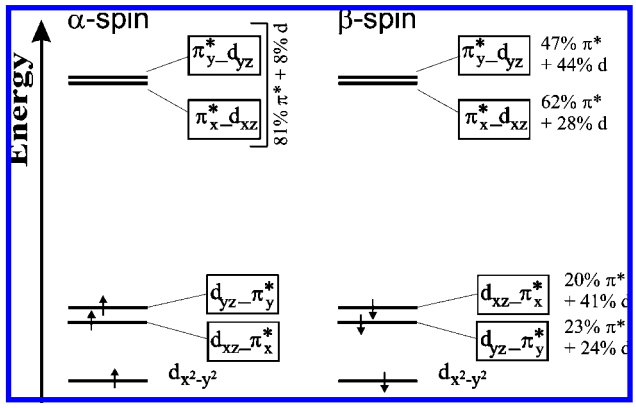

show a d orbital contribution of only 8%, compared to 27% for the Fe(II)−NO^+ state. As mentioned above, the unpaired electrons in the LS Fe(III)−NO(radical) case are primarily located in α-d_{yz} and β-π_y*. The latter orbital is strongly mixed with β-d_{yz}, leading to a corresponding antibonding combination that consists of 47% π_y* and 44% β-d_{yz}. This strong covalency quenches part of the spin density, leading to a distribution of roughly +0.5 on Fe and −0.5 on NO. The remaining backbond between β-d_{xz} and β-π_x* is comparable to that of the Fe(II)−NO^+ state (see Scheme 2), and hence shows a strong contribution to the total spin density, resulting in the calculated values listed above. In summary, although one of the β-spin back-bonds is strengthened, this is not sufficient to compensate for the loss of α-spin back-bonding. This explains the distinctively weaker Fe−NO bond in the LS Fe(III)−NO(radical) case, for which ν(Fe−NO) is predicted to be only 430 cm^{-1} (Table 4) with an Fe−NO force constant of 2.26 mdyn/Å (Table 5). For ν(N−O), a shift of ∼70 cm^{-1} to lower energy is predicted because of the formal electron transfer from iron to the π* antibonding orbitals of NO in this case. The observation that the Fe−N−O unit is not bent in the LS Fe(III)−NO(radical) state is due to the fact that the coupling of the ^{2}E state from $[d_{xz},d_{yz}]^3$ on iron with the ^{2}E state from $[\pi_x,\pi_y]^3$ on NO leads to nondegenerate states, even in an effective C_{4v} symmetry. The resulting electronic state is therefore not Jahn−Teller-active. In conclusion, a crossing from the Fe(II)−NO^+ ground state to the LS Fe(III)−NO(radical) state is induced by an elongation of the Fe−NO bond and leads to a distinct weakening of the Fe−NO and N−O bonds. The closeness in energy of these states implies that there might be some LS Fe(III)−NO(radical) admixture into the Fe(II)−NO^+ ground state. This mixing could be dynamically mediated by the Fe−NO stretch, which means that the Fe(II)−NO^+ ground state and the LS Fe(III)−NO(radical) state would become vibronically coupled. In C_{4v} symmetry, coupling between the $^1A_1$ ground state of Fe(II)−NO^+ with the $^1A_1$ component of LS Fe(III)−NO(radical) could indeed be induced by ν(Fe−NO).[52]

On the basis of these findings, the dissociation of NO from the ferric iron center could be envisioned as follows: Upon a small elongation of the Fe−NO bond to ∼1.70 Å (see Figure 7), the critical electron transfer that leads from the Fe(II)−NO^+ state to the LS Fe(III)−NO(radical) electronic structure, which is a symmetry-allowed process, takes place. If NO moves farther away from the iron, the LS Fe(III)−NO(radical) PES crosses the HS Fe(III)−NO(radical) PES (shown in black in Figure 7), which corresponds to the electronic state where high-spin Fe(III) is antiferromagnetically coupled to the unpaired electron of NO. Hence, this process is identical with a spin crossover of the Fe(III) center from low-spin to high-spin. The HS Fe(III)−NO(radical) state corresponds to the product state that is obtained after complete dissociation of NO, because 5C ferric heme is known to be high-spin. The crossing of these surfaces is roughly predicted to occur at ∼1.9 Å and hence, still at an Fe−NO distance below 2 Å. These two states cannot directly interact by spin−orbit coupling, so the intersystem crossing must be mediated by intermediate $S = 1$ states, but we have not investigated this point further. In summary, *the major finding of these PES calculations on 6C ferric heme NO adducts is that upon an elongation of the Fe−NO bond of only ∼0.25 Å, the complex passes through at least three different electronic states* (plus at least one intermediate $S = 1$ state). The observed complexity of this energy landscape is unprecedented, even for transition-metal nitrosyls.

Discussion

In this work, the new six-coordinate (6C) Fe(III)−porphyrin NO model complex [Fe(TPP)(MI)(NO)](BF_4) (**1**) was prepared from [Fe(TPP)(BF_4)] by careful reaction with purified NO. The structure of the bis(thf)-coordinated precursor has been determined. Complex **1** was used to explore the spectroscopic properties and electronic structures of 6C ferric heme nitrosyl model complexes using IR and, for the first time, nuclear resonance vibrational spectroscopy (NRVS) along with normal coordinate analysis (NCA) and DFT calculations. For complex **1**, N−O and Fe−NO stretching frequencies of 1896 and 580 cm^{-1} (578 cm^{-1} measured with ^{57}Fe), respectively, are assigned using isotope labeling. From NCA, force constants of 15.18 and 3.92 mdyn/Å for the N−O and Fe−NO bonds, respectively, are determined for complex **1**. The electronic structure of this complex is in agreement with the widely accepted Fe(II)−NO^+ description for ferric nitrosyls, as reflected by the N−O stretching frequency of ∼1900 cm^{-1} and the linear Fe−N−O unit observed in crystal structures of closely related model complexes.[8a,11] The Fe−NO interaction in ferric heme is dominated by strong π back-bonding between two d_π orbitals of the metal and two empty π* orbitals of NO^+. This leads to a net transfer of one electron from the metal to the ligand and explains the decrease of the N−O stretching frequency from 2390 cm^{-1} in free NO^+ to ∼1900 cm^{-1} in complex **1**. In contrast, the Fe−NO σ interaction in ferric heme is weak, as a result of the generally poor donor abilities of the σ_{nb} orbital in diatomics with multiple bonds. In accord with this strong π/weak σ bonding description, the Fe−N−O unit is linear and short to maximize the π interactions. Recently, it was proposed that the ferric heme NO adducts in nitrophorins might have an electronic structure that corresponds to Fe(III)−NO(radical) in order to prevent autoxidation.[53,6c] However, the experimental data available for ferric heme NO adducts with axial N-donor coordination in proteins and model complexes show that these species have

(52) It should be noted that the symmetry of 6C ferric heme nitrosyls is lower than C_{4v}, which further diminishes symmetry-related restrictions. C_{4v} is the maximum possible symmetry of a corresponding 5C $[Fe(porphyrin)(NO)]^+$ complex.

(53) In the case of the nitrophorins, it has been proposed that the ruffled conformation of heme plays a major role in stabilizing a $[d_{xz}^2d_{yz}^2d_{xy}^1]$-type ground state. This could lead to the formation of a corresponding ferric heme nitrosyl in the LS Fe(III)−NO(radical) state where the unpaired electron is localized in the d_{xy} orbital (see the Introduction). This is different from the LS Fe(III)−NO(radical) form invoked here, where the unpaired electron is localized in the d_{yz} orbital.

the assumed Fe(II)−NO^+ ground state (on the basis of Fe−NO bond distances and Fe−NO and N−O stretching frequencies). For example, the N−O stretching frequency of 1917 cm^{-1} for ferric rNp1−NO is very close to the values obtained for model complex **1** and corresponding enzymatic species (see Table 1). Hence, this indicates that the electronic structures of ferric nitrophorin NO adducts do not differ from those of the other ferric nitrosyl species. In summary, a very detailed picture of the electronic properties of the Fe(II)−NO^+ electronic ground state of these complexes has now emerged.

The quantitative description provided here for the Fe−NO bond in the ferric heme complex **1** makes possible a detailed comparison with the corresponding ferrous complex [Fe(TPP)(MI)(NO)] (**3**) studied previously.[21a,b] Interestingly, the one-electron reduction of the Fe(II)−NO^+ complex **1** is mostly ligand-centered, resulting in an Fe(II)−NO(radical) electronic structure description of **3**. This is evident from the N−O stretching frequency, which is reduced from 1896 cm^{-1} in **1** to 1630 cm^{-1} in **3**. The Fe−NO bond in the ferrous complex corresponds to a σ bond mediated by the singly occupied π^* orbital of NO and the d_{z^2} orbital of iron along with a π back-bond between the unoccupied π^* orbitals of NO and the d_π orbitals of the metal.[21b] The strong σ bond explains both the large stability of the Fe−NO bond in this case and the observed *trans* effect of the NO ligand on axially coordinated N-donor ligands, which induces long Fe(II)−$N_{imidazole}$ bond lengths compared to the corresponding bis(imidazole)-ligated Fe(II)−porphyrins.[54] In contrast, the σ bond is clearly much weaker in **1** because it is mediated by the low-lying orbital σ_{nb}. Hence, this difference in σ bonding explains the very short Fe−NO bond in **1** and the lack of a significant *trans* effect of NO in ferric heme NO adducts. In fact, all Fe(II)−NO^+ complexes with *trans* N-donor ligands exhibit Fe−$N_{imidazole}$ bond lengths comparable to those of the corresponding $[Fe^{III}(porphyrin)(imidazole)_2]^+$ complexes.[14a] On the other hand, the overall π back-bond is stronger in **1**.[55] When these contributions are summed up, one would expect a somewhat stronger Fe−NO bond in ferrous hemes because of the stronger σ bond. *In contrast to this prediction, the actual experimental difference in Fe−NO bond strengths in these systems is much more dramatic: experimental complex formation constants (K_{eq}) of ferrous compared to ferric heme nitrosyls differ in general by 4−5 orders of magnitude* (~6 orders of magnitude in the case of the nitrophorins[56]). This trend is nicely reproduced by the calculated free energies of complex formation, $\Delta G°$, given in Table 7. In the case of the 6C ferric complex **1**, the obtained formation energy is only about −4 kcal/mol. The magnitude of this value is at the low end of the experimentally determined values, which range from −4 to −7 kcal/mol ($K_{eq} = 10^3-10^5$ M^{-1}) for ferric heme nitrosyls. In comparison, the Fe−NO bond is predicted to be thermodynamically stronger by 7.5 kcal/mol for the corresponding 6C ferrous complex, which is again in reasonable agreement with experiment ($K_{eq} = 10^{11}-10^{12}$ M^{-1}, corresponding to $\Delta G°$ in the range from −15 to −16 kcal/mol). This dramatic increase in the Fe−NO bond strength in going from the ferric to the ferrous case is not in agreement with the difference in MO bonding descriptions elaborated above. In addition, this trend is also not in agreement with the observed trend in force constants: **1** has a much larger Fe−NO force constant (3.92 mdyn/Å) than **3** (2.38 mdyn/Å). Therefore, we still lack a fundamental understanding of the Fe−NO interaction in the ferric heme complexes. This becomes evident from a detailed evaluation of the potential energy surfaces (PES) of the different electronic states of **1**.

Scheme 3. Ground State PES, Taking into Account the Relative Error of ~2 kcal/mol in the DFT Energies

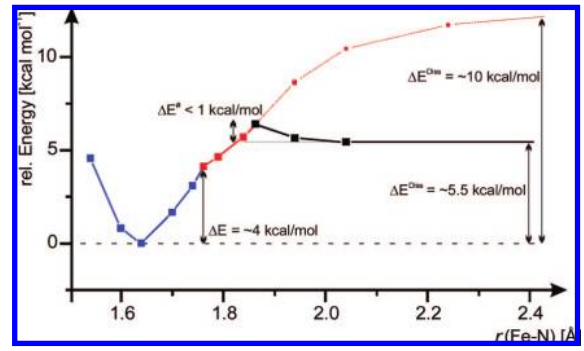

In order to obtain detailed insight into the Fe−NO interaction in 6C ferric heme nitrosyls, we calculated the PES for three key electronic states, as shown in Figure 7: (a) Fe(II)−NO^+ ($S = 0$, blue curve), which is the established ground state as described above; (b) the open-shell singlet state low-spin (LS) Fe(III)−NO(radical), where LS Fe(III) is antiferromagnetically coupled to NO ($S = 0$, red curve); and (c) the corresponding state high-spin (HS) Fe(III)−NO(radical) ($S = 2$, black curve), which corresponds to the product state upon dissociation of NO. *These results show that the elusive LS Fe(III)−NO(radical) state does in fact exist as an energy minimum and that this state is surprisingly close in energy to the Fe(II)−NO^+ ground state* (with a DFT energy separation of only ~1 kcal/mol). It is likely that the calculated energy difference between these states is underestimated by a few kilocalories per mole, at least for the case of axial N-donor coordination. This is evident from the vibrational properties, which do not show any indication of the presence of the LS Fe(III)−NO(radical) state. From the calculated complex formation energies, a realistic error of 1−2 kcal/mol is estimated for the B3LYP/TZVP method. This would shift the crossing point of the two $S = 0$ surfaces to about 1.70−1.76 Å. In addition, the two states could be mixed, so the shape of the ground-state PES around the crossing point is clearly not well-defined by the DFT treatment. Scheme 3 shows the ground-state PES with corrected energies as an illustration, including key energy parameters. When the small error in relative energies from DFT is taken into account, it is estimated that an Fe−NO bond elongation of only 0.05−0.1 Å from the equilibrium position leads to a change in ground state, i.e. the critical iron(II)-to-NO^+ electron transfer occurs at an Fe−NO distance of only 1.70−1.75 Å. Importantly, the properties of the Fe(II)−NO^+ and LS Fe(III)−NO(radical) states are very different. From the calculations, the LS Fe(III)−NO(radical) state has a weaker (longer) Fe−NO bond and hence, a lower Fe−NO stretching frequency. Because of the electron transfer from Fe(II) into a π^* orbital of NO^+, the N−O bond is also weaker, shifting ν(N−O) to lower frequency. Hence, both the

(54) Wyllie, G. R. A.; Schulz, C. A.; Scheidt, W. R. *Inorg. Chem.* **2003**, *42*, 5722–5734.

(55) Interestingly, this actually relates not to the observed π^*_d mixing but only to the fact that the number of back-bonds is reduced from 2 in **1** to 1.5 in **3**. This is evident from the d orbital contributions to the corresponding π^*_d antibonding orbitals, which are 27% for **1** and 25% (average) for **3** for the π_y^*_d_{yz} orbital (α/β<126> in ref 21b). This indicates that the linear Fe−N−O unit and the shorter Fe−NO bond alone do *not* facilitate the π back-bond in **1** as compared to **3**.

(56) Berry, R. E.; Ding, X. D.; Shokhireva, T. K.; Weichsel, A.; Montfort, W. R.; Walker, F. A. *J. Biol. Inorg. Chem.* **2004**, *9*, 135–144.

Fe−NO and N−O bonds become weaker in going from Fe(II)−NO^+ to LS Fe(III)−NO(radical), which corresponds to a direct correlation of these bond strengths.

These results are very important, as they imply that a small perturbation of the Fe−N−O unit (due to interaction of the bound NO with a protein side chain, for example) might be able to induce a change of the ground state from Fe(II)−NO^+ to LS Fe(III)−NO(radical). This should be evident from the spectroscopic properties of the complex. However, no clear experimental proof for the existence of a ferric heme nitrosyl with the LS Fe(III)−NO(radical) ground state is available to date. Nevertheless, this finding offers an attractive explanation for the observed weaker Fe−NO and N−O bond strengths in ferric heme nitrosyls with axial thiolate coordination, which could be attributed to a change in ground state to LS Fe(III)−NO(radical). However, this would not explain the observed bending of the Fe−N−O unit; our results demonstrate that a bent Fe−N−O unit is not an intrinsic property of the LS Fe(III)−NO(radical) state. On the other hand, recent DFT results show that all of these properties of thiolate-coordinated ferric heme nitrosyls can also be explained within the Fe(II)−NO^+ ground-state model.[19] This point needs further investigation.

Upon a further elongation of the Fe−NO bond, the LS Fe(III)−NO(radical) crosses the HS Fe(III)−NO(radical) PES at a distance of ∼1.9 Å (see Scheme 3). This transition corresponds to a spin crossover of Fe(III) and is related to the fact that the five-coordinate (5C) ferric heme product is actually high-spin. Importantly, *the HS Fe(III)−NO(radical) PES is dissociative for the Fe−NO bond*. This generates a small kinetic barrier for the dissociation of NO, which, however, is <1 kcal/mol and hence negligible. More importantly, this dramatically lowers the thermodynamic stability of the ferric Fe−NO bond, from about −10 kcal/mol on the LS surfaces to only about −4 kcal/mol (Scheme 3). Therefore, *the properties of the HS Fe(III)−NO(radical) PES determine the thermodynamic weakness of the Fe−NO bond and the large dissociation rate constant of NO in ferric heme nitrosyls*. This means that once the system has entered the HS Fe(III)−NO(radical) electronic state, the dissociative nature of this PES will actually drive the NO away from the metal center, allowing the NO to diffuse off and inhibiting its retention. This explains the surprisingly large rate constants for NO dissociation measured experimentally for ferric hemes. On the other hand, the large Fe−NO force constant and short Fe−NO distance in the ground state relate to the properties of the Fe(II)−NO^+ surface, which is very steep as a result of the fact that the dissociation of the complex into Fe(II) and NO^+ is energetically very unfavorable. For this reason, the experimentally derived Fe−NO force constant is *not* a measure of the stability of the Fe−NO bond in this case. *These quantities are actually completely unrelated because they depend on the properties of different electronic states*. Because of this, complex **1** has a large Fe−NO force constant but actually a quite weak Fe−NO bond, in agreement with the small NO binding constant and the observed rapid loss of NO from the iron center in solution. Altogether, dissociation of NO from the ferric iron center requires the system to pass through at least three different electronic states (plus an $S = 1$ intermediate state). The observed complexity of this energy landscape is unprecedented, even for transition-metal nitrosyls. The "simple" Fe(II)−NO^+ description of the electronic structure of these complexes, and the analogies normally drawn to Fe(II)−heme CO complexes, do not in any way implicate such complexity as determined here.

On the basis of these properties of ferric heme nitrosyls, the occurrence of ferric instead of ferrous hemes in the NO delivery proteins (nitrophorins) and enzyme−product complexes of cytochrome cd_1 NiR and NOS is not arbitrary. This is actually related to the weakness of the Fe−NO bond in the ferric systems, which enables loss of NO. The corresponding rate constants k_{off} are about 4−8 orders of magnitude larger in ferric than in ferrous hemes, as discussed above.[2g,57] Hence, formation of ferrous heme NO adducts has often been called a "dead end" for protein activity and would certainly impose a rather dramatic limit on the dissociation of NO from the NiR or NOS enzyme−product complexes or the nitrophorins.

Finally, it is interesting to compare the properties of ferric heme nitrosyls to those of the corresponding Ru(III)−NO adducts. In the latter case, the electronic structure also corresponds to Ru(II)−NO^+, but no lability of the bound NO is observed. On the contrary, these compounds are some of the most stable transition-metal nitrosyls known. What is the reason for this substantial difference? Since ruthenium is a second-row transition metal, its tendency to form high-spin complexes is greatly reduced. Hence, 5C Ru(III) products obtained upon dissociation of NO from the corresponding nitrosyl complexes in general have low-spin ground states, and therefore, no spin crossover is observed upon loss of NO. In view of Figure 7, this would mean that the HS metal(III)−NO(radical) energy surface (black) disappears (i.e., shifts to much higher energy) for Ru(III). Independently of how the energies of the $S = 0$ states play out, the removal of the HS metal(III)−NO(radical) surface from the picture automatically leads to a much more stable complex. This is another demonstration of how significant these results are for the detailed understanding of the electronic structures, thermodynamic stabilities, spectroscopic properties, and reactivities of group 8 metal(III) nitrosyls.

Conclusions

In this study, we have characterized the Fe(II)−NO^+ ground state of six-coordinate ferric heme nitrosyls in detail using the model complex [Fe(TPP)(MI)(NO)](BF_4) as an example. Through the use of DFT calculations, the elusive low-spin Fe(III)−NO(radical) ($S = 0$) state has then been investigated. Surprisingly, this state is located just a few kilocalories per mole above the ground state. It is characterized by properties very different from those of Fe(II)−NO^+; in particular, the Fe−NO and N−O bond strengths are greatly reduced as a result of the reduction of π back-bonding. Upon a small (0.05−0.1 Å) elongation of the Fe−NO bond from the equilibrium position, the Fe(II)−NO^+ ground-state potential energy surface (PES) crosses the low-spin Fe(III)−NO(radical) ($S = 0$) energy surface. Importantly,

(57) Ford, P. C.; Laverman, L. E. *Coord. Chem. Rev.* **2005**, *249*, 391–403.
(58) Suzuki, N.; Higuchi, T.; Urano, Y.; Kikuchi, K.; Uchida, T.; Mukai, M.; Kitagawa, T.; Nagano, T. *J. Am. Chem. Soc.* **2000**, *122*, 12059–12060.
(59) Hu, S.; Kincaid, J. R. *J. Biol. Chem.* **1993**, *268*, 6189–6193.
(60) Tomita, T.; Haruta, N.; Aki, M.; Kitagawa, T.; Ikeda-Saito, M. *J. Am. Chem. Soc.* **2001**, *123*, 2666–2667.
(61) Pinakoulaki, E.; Gemeinhardt, S.; Saraste, M.; Varotsis, C. *J. Biol. Chem.* **2002**, *277*, 23407–23413.
(62) Wang, J.; Lu, S.; Moënne-Loccoz, P.; Ortiz de Montellano, P. R. *J. Biol. Chem.* **2003**, *278*, 2341–2347.
(63) (a) Sampath, V.; Zhao, X.; Caughey, W. S. *Biochem. Biophys. Res. Commun.* **1994**, *198*, 281–287. (b) Wang, Y.; Averill, B. A. *J. Am. Chem. Soc.* **1996**, *118*, 3972–3973.
(64) Miller, L. M.; Pedraza, A. J.; Chance, M. R. *Biochemistry* **1997**, *36*, 12199–12207.

this shows that the low-spin Fe(III)−NO(radical) ($S = 0$) state could become the ground state of ferric heme nitrosyls upon small steric or electronic perturbations that may occur in protein active sites. This is especially true for axial thiolate (cysteinate) coordination, because thiolates tend to stabilize Fe(III). The observed thermodynamic weakness of the Fe−NO bond in ferric heme nitrosyls is due to the properties of the high-spin Fe(III)−NO(radical) ($S = 2$) state, which is dissociative with respect to the Fe−NO bond. These PES calculations reveal an unexpectedly complex energy landscape for binding of NO to ferric heme.

Acknowledgment. The Advanced Photon Source is supported by the DOE, Basic Energy Sciences, Office of Science, under Contract DE-AC02-06CH11357. S.D.G. acknowledges SSRL for funding. SSRL operations are funded by the Department of Energy, Office of Basic Energy Sciences. The Structural Molecular Biology program is supported by the National Institutes of Health, National Center for Research Resources, Biomedical Technology Program, and by the Department of Energy, Office of Biological and Environmental Research. This work was supported by the Deutsche Forschungsgemeinschaft (DFG) (Grant LE 1393/1-2). F.P. acknowledges the Fonds der Chemischen Industrie (FCI) for a Chemiefonds fellowship.

Supporting Information Available: Complete ref 35, vibrational spectra of [Fe(TPP)(NO)(NO_2)] (including the $^{15}N^{18}O$-labeled compound), NRVS raw data, IR spectra of NRVS samples, the PES obtained using B3LYP/LANL2DZ, MO diagrams for porphine dianion (P^{2-}) and NO, Cartesian coordinates of DFT-optimized structures, and crystallographic data for [Fe(TPP)($thf)_2$](BF_4) in CIF format. This material is available free of charge via the Internet at http://pubs.acs.org.

JA801860U